Cobalt- and Rhodium-Corrole-Triphenylphosphine Complexes Revisited: The Question of a Noninnocent Corrole

Sumit Ganguly,[a] Diemo Renz,[a] Logan J. Giles,[b] Kevin J. Gagnon,[c] Laura J. McCormick,[c] Jeanet Conradie,[d] Ritimukta Sarangi*,[b] and Abhik Ghosh*,[a]

[a]Department of Chemistry, UiT – The Arctic University of Norway, N-9037 Tromsø, Norway;
[b]Structural Molecular Biology, Stanford Synchrotron Radiation Lightsource,
SLAC National Accelerator Laboratory, Menlo Park, CA, 94306, USA
[c]Advanced Light Source, Lawrence Berkeley National Laboratory,
Berkeley, CA 94720-8229, USA
[d]Department of Chemistry, University of the Free State, 9300 Bloemfontein,
Republic of South Africa

Email: ritis@slac.stanford.edu (RS), abhik.ghosh@uit.no (AG)

Note! The crystal structures described in this paper have been deposited at the Cambridge Crystallographic Data Centre and assigned the deposition numbers 1535564-1535566.

Abstract. A reinvestigation of cobalt-corrole-triphenylphosphine complexes has yielded an unexpectedly subtle picture of their electronic structures. UV-vis absorption spectroscopy, skeletal bond length alternations observed in X-ray structures, and broken-symmetry DFT (B3LYP) calculations suggest partial Co^{II}-$corrole^{\bullet 2-}$ character for these complexes. The same methods applied to the analogous rhodium corroles evince no evidence of a noninnocent corrole. X-ray absorption spectroscopic studies showed that the Co K rising edge of Co[TPC](PPh_3) (TPC = triphenylcorrole) is redshifted by ~1.8 eV relative to the *bona fide* Co(III) complexes Co[TPC]$(py)_2$ and Co[TPP](py)Cl (TPP = tetraphenylporphyrin, py = pyridine), consistent with a partial Co^{II}-$corrole^{\bullet 2-}$ description for Co[TPC](PPh_3). Electrochemical measurements have shown that both the Co and Rh complexes undergo two reversible oxidations and 1-2 irreversible reductions. In particular, the first reduction of the Rh corroles occurs at significantly more negative potentials than that of the Co corroles, reflecting significantly higher stability of the Rh(III) state relative to Co(III). Together, the results presented herein suggest that cobalt-corrole-triphenylphosphine complexes are significantly noninnocent with moderate Co^{II}-$corrole^{\bullet 2-}$ character, underscoring – yet again – the ubiquity of ligand noninnocence among first-row transition metal corroles.

Introduction. Half a century after the term was coined,[1] noninnocent ligands continue to fascinate inorganic chemists.[2,3] Not only have important new examples of such ligands emerged in recent years, they have also been recognized for their important role in redox catalysis.[4] The phenomenon is particularly widespread in the currently fast-developing field of metallocorroles, where a large number of complexes exhibit varying degrees of corrole$^{\bullet 2-}$ character.[5] Thus, while copper[6,7,8,9,10,11,12,13,14,15] and chloroiron[7,16,17,18] corroles were recognized as noninnocent early on, new examples of noninnocent metallocorrole systems such as FeNO[19,20] and $Fe_2(\mu\text{-}O)$[21] corroles are also accumulating at a steady rate.[22] (Examples of innocent metallocorroles include CrO and MoO corroles,[23] TcO[24] and ReO[25] corroles, RuN[26] and OsN[27] corroles, and Au[28,29,30] corroles.) In this study, we have evaluated the potential noninnocent character of cobalt-corrole-triphenylphosphine[31,32,33] complexes and compared them with their rhodium analogues.[34,35] The question is an important one, because cobalt corroles are of increasing importance in a number of technological applications such as hydrogen evolution from water[36,37,38] and ligand sensing.[39,40,41,42]

As in a number of other cases, the first inkling that Co-PPh_3 corroles may not be true Co(III) complexes came from their optical spectra. Over a long series of studies,[5-7,10-16,19-30] we have established that the Soret absorption maxima of noninnocent *meso*-tris(*para*-X-phenyl)corrole (T*p*XPC) derivatives redshift markedly with increasingly electron-donating character of the *para* substituent X. The Soret maxima of innocent metallotriarylcorroles, in contrast, do not exhibit such a sensitivity to X. An examination of the literature readily established that the Soret maxima of Co[T*p*XPC](PPh_3) redshift significantly in response to increasingly electron-donating X groups.[32,33] Accordingly, we undertook a comprehensive reinvestigation of these complexes, employing UV-vis spectroscopy, electrochemistry, X-ray absorption and emission spectroscopies (XAS, XES), and DFT calculations. For comparison, we also investigated the β-octabrominated cobalt series Co[Br_8T*p*XPC](PPh_3) and the rhodium series Rh[T*p*XPC](PPh_3). Together, the results paint a remarkably subtle picture of the electronic structure of these complexes, as described below.

Results and discussion. **(a) Synthesis and proof of composition**. Figure 1 depicts the three series of compounds investigated herein. For the Co[T*p*XPC](PPh_3) series, four of the five complexes investigated (X = NO_2, H, Me, and OMe) have been previously reported and were resynthesized for this study.[32,33] The Co[Br_8T*p*XPC](PPh_3) series, except for Co[Br_8TPC](PPh_3) (TPC = triphenylcorrole),[43] and the Rh[T*p*XPC](PPh_3) series both consist of new compounds.

The synthetic protocols ranged from modifications of literature procedures to essentially new procedures, as described below.

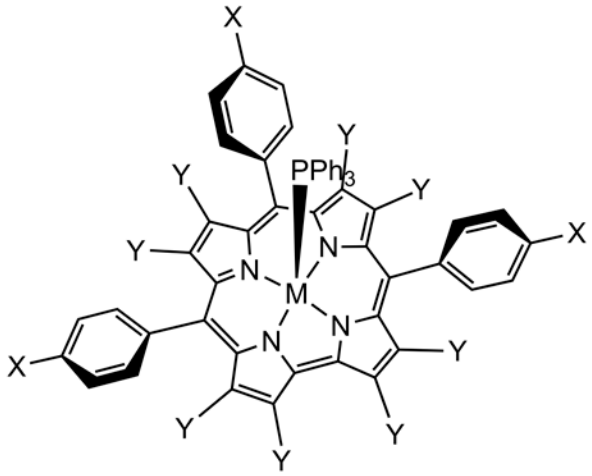

Series	X	Y
Co[T*p*XPC](PPh$_3$)	NO_2, CF_3, H, Me, OMe	H
Co[Br$_8$T*p*XPC](PPh$_3$)	CF_3, H, Me, OMe	Br
Rh[T*p*XPC](PPh$_3$)	CF_3, H, Me, OMe	H

Figure 1. Complexes investigated in this study.

Cobalt insertion into corroles has traditionally been accomplished in alcoholic solvents, particularly such as methanol, in the presence of the axial ligand.[31,32,32,33 ,44,45,46] Several of the free-base corroles needed in this study, including H$_3$[T*p*XPC] (X ≠ CF_3) and all H$_3$[Br$_8$T*p*XPC] ligands, however, were found to be poorly soluble in methanol. The use of THF avoided the solubility problems and complete Co insertion took place smoothly at 45-50 °C in about 90 min for both the T*p*XPC and Br$_8$T*p*XPC series.

For the rhodium corroles reported here, an essentially new synthetic protocol was devised. A first attempt, inspired by a similar method used by Gray *et. al.*[47] for the preparation of iridium-tris(pentafluorophenyl)corrole-PPh$_3$, involved the reaction of free base triarylcorroles with an excess of [Rh(cod)$_2$Cl]$_2$ in refluxing THF under an inert atmosphere and in presence of excess PPh$_3$ and dry K_2CO_3. Except for X = CF_3, however, this procedure failed for all the other free base H$_3$[T*p*XPC] ligands. Fortunately, changing the solvent to 2:1 dichloromethane/ethanol and using much smaller quantities of both the metal source (1.5 equiv) and PPh$_3$ (1 equiv) provided facile access to all four Rh[T*p*XPC](PPh$_3$) complexes at room temperature and without any provision for an inert atmosphere. Somewhat similar conditions (albeit with no ethanol) have

also been previously used by Collmann *et al*. for the synthesis of various Rh-corrole-amine complexes.[48]

Proof of purity and composition of the products came from clean thin-layer chromatograms, ESI-MS, fully assigned diamagnetic ^{1}H NMR spectra, elemental analyses for all new compounds that withstood warming and rigorous drying, and, for three compounds, single-crystal X-ray structures.

(b) Single-crystal X-ray structures. Because several X-ray structures have already been reported for Co-triarylcorrole-PPh_3 complexes,[44,45,46,53,54,**Error! Bookmark not defined.**] no attempt was made to crystallographically characterize the Co[T*p*XPC](PPh_3) series. X-ray structures were obtained for the novel β-octabrominated complex Co[Br_8T*p*CF_3PC](PPh_3), and for two Rh corroles, Rh[TPC](PPh_3) and Rh[T*p*OMePC](PPh_3). Figure 2 presents graphical representations of the three structures and Tables 1 and 2 list key crystallographic data and geometrical parameters, respectively. A summary of pertinent structural data from the literature is given in Table 3.

The Co-N and Rh-N bond distances in the structures obtained here are in good accord with literature values (Table 3).[49] The Co-N distances (~1.88 ± 0.01 Å) are about 0.08-0.09 Å shorter than the Rh-N distances (~1.965 ± 0.01 Å), which is somewhat smaller than the differences in Shannon-Prewitt ionic radii for the two low-spin M(III) ions (Co 54.5 Å, Rh 66.5 Å)[50,51] and in Pyykkö's single-bond covalent radii (Co 1.11 Å, Rh 1.25 Å).[52] Comparison with non-corrole X-ray structures suggests that these discrepancies largely reflect unusually short Rh-N distances in Rh corroles, evidently a result of the sterically constricted nature of the corrole N_4 cavity. Careful examination of the M-N_4, M-$C_{\alpha 8}$, and M-$C_{\beta 8}$ displacements and saddling dihedrals shows that the macrocycle conformation is planar to slightly saddled for the majority of the Co complexes and mildly domed for the Rh complexes (Table 3). Both the Co and Rh corroles, however, exhibit similar M-N_4 out-of-plane distances, ~0.26-0.28 Å for Co and ~0.27-0.31 Å for Rh.[35,45] The crystal packing of the complexes varies; thus, both partially cofacial dimers (e.g., Figure 2b) and unstacked (e.g., Figure 2e) are observed for different complexes.

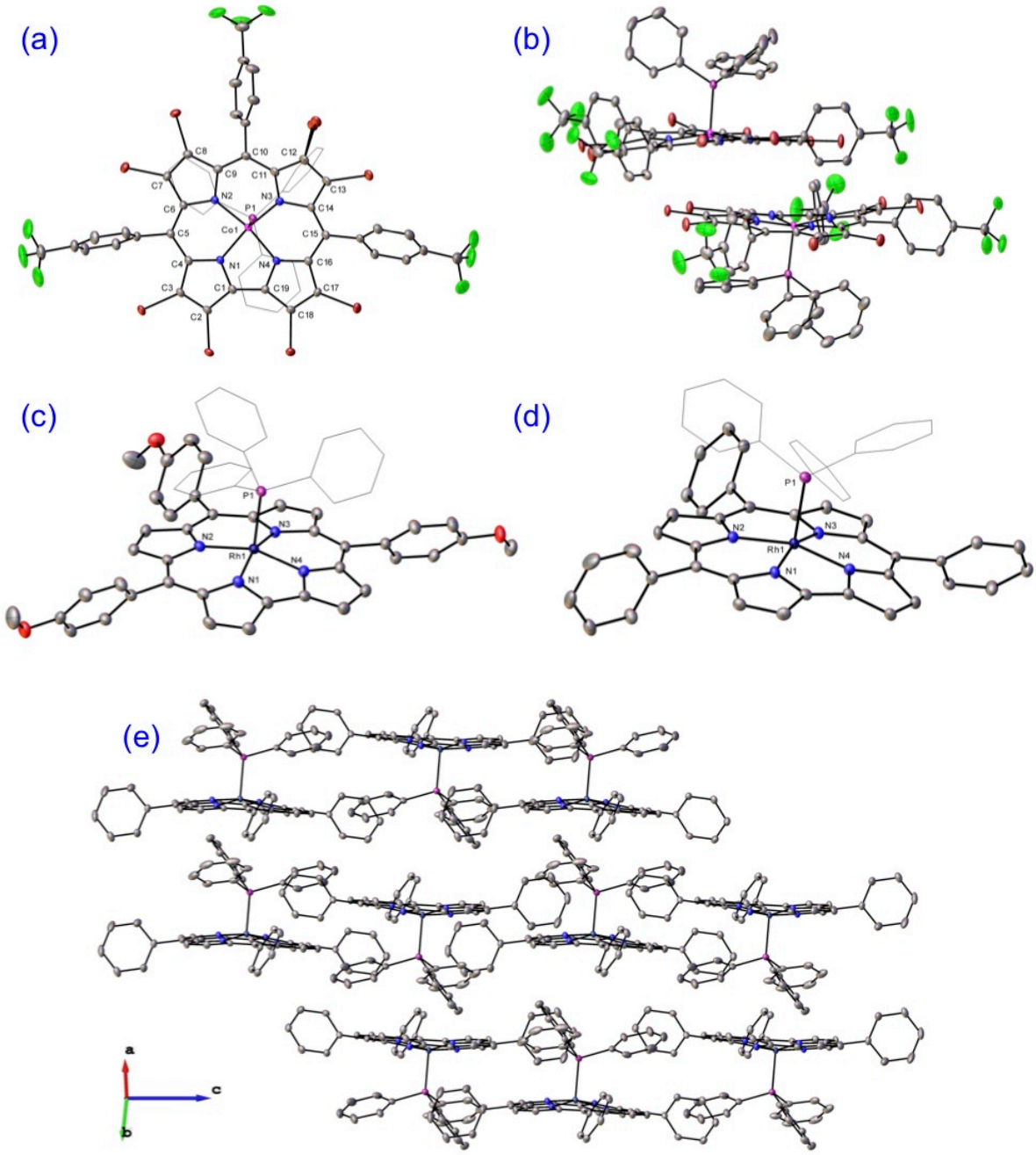

Figure 2. Selected views of X-ray structures. Co[Br_8T*p*CF_3PC](PPh_3): (a) top and (b) side views; (c) Rh[T*p*OMePC](PPh_3); Rh[TPC](PPh_3): (d) single molecule and (e) packing diagram.

The Table 1. Crystallographic data for Co[Br_8T*p*CF_3PC](PPh_3), Rh[TPC](PPh_3), and Rh[T*p*OMePC](PPh_3).

Sample	Co[Br_8T*p*CF_3PC](PPh_3)	Rh[TPC](PPh_3)	Rh[T*p*OMePC](PPh_3)
Chemical formula	$C_{58}H_{27}F_9Br_8N_4PCo$	$C_{55}H_{38}N_4PRh$	$C_{58}H_{44}O_3N_4PRh$
Formula mass	1680.01	888.77	978.85
Crystal system	Monoclinic	Triclinic	Monoclinic
Space group	*C*2/*c*	*P*-1	$P2_1/c$
λ (Å)	0.7749	0.7749	0.7749
a (Å)	19.9698(12)	8.5019(4)	12.1715(4)
b (Å)	23.7533(13)	13.1646(7)	20.0064(7)
c (Å)	28.7932(15)	18.1789(9)	18.2451(6)
α (deg.)	90	94.102(3)	90
β (deg.)	96.104(3)	92.306(3)	98.228(2)
γ (deg.)	90	97.775(3)	90
Z	8	2	4
V (Å^3)	13580.6(13)	2008.22(17)	4397.1(3)
Temperature (K)	100(2)	100(2)	100(2)
Density (g/cm^3)	1.643	1.470	1.479
Measured reflections	134476	30310	84124
Unique reflections	24858	14381	16042
Parameters	734	550	607
Restraints	1	0	0
R_{int}	0.045	0.0625	0.0547
θ range (deg.)	2.213 – 36.070	2.178 – 35.825	2.152 – 36.001
R_1, wR_2 all data	0.0355/0.0845	0.0512/0.0982	0.0416/0.1030
S (GooF) all data	1.066	1.037	1.034
Max/min res. dens. (e/Å^3)	1.144/-1.048	1.189/-1.417	1.976/-0.650

Table 2. Selected crystallographic geometry parameters (Å) for Co[Br_8T*p*CF_3PC](PPh_3), Rh[TPC](PPh_3), and Rh[T*p*OMePC](PPh_3).

Distances	Co[Br_8T*p*CF_3PC](PPh_3)	Rh[TPC](PPh_3)	Rh[T*p*OMePC](PPh_3)
M(1)-N(1)	1.8758(17)	1.9437(18)	1.9572(17)
M(1)-N(2)	1.9026(17)	1.9691(18)	1.9730(17)
M(1)-N(3)	1.8940(17)	1.9724(18)	1.9643(16)
M(1)-N(4)	1.8838(17)	1.9499(19)	1.9443(17)
M(1)-P(1)	2.2248(6)	2.2098(6)	2.2150(5)
M(1)-4N_{plane}	0.2623(10)	0.2788(10)	0.3171(9)

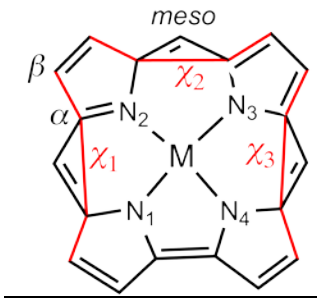

Table 3. Comparison of key distances (Å) and dihedrals ($\chi_1 - \chi_3$) for Co/Rh-corrole-PPh_3 complexes reported in the literature.

Complex	CCSD	d(M-$N_{1/4}$)$_{ave}$	d(M-$N_{2/3}$)$_{ave}$	d(M-P)	d(M-N_4)	d(M-$C_{\alpha 8}$)	d(M-$C_{\beta 8}$)	χ_1	χ_2	χ_3	Conformation	ref
Co[TPFPC](PPh_3)[a]	BAQPUF	1.872	1.886	2.205	0.262	0.309	0.375	1.5	18.3	7.4	planar	44
Co[TPC](PPh_3)	KIMQOM	1.866	1.889	2.201	0.280	0.361	0.471	1.2	20.6	22.6	planar	44
Co[T2,4Cl_2PC](PPh_3)[b]	SUCMOU (molecule 1)	1.866	1.880	2.217	0.289	0.341	0.437	4.8	11.0	6.0	planar	53
Co[T2,4Cl_2PC](PPh_3)[b]	SUCMOU (molecule 2)	1.866	1.880	2.216	0.289	0.360	0.477	2.4	5.2	16.3	planar	53
Co[T2ClPC](PPh_3)[c]	CAHJIH	1.868	1.882	2.204	0.286	0.384	0.523	0.2	17.5	22.3	slightly domed	54
Co[TDFPC](PPh_3)[d]	CAJKEG	1.868	1.890	2.205	0.277	0.373	0.507	0.6	19.1	22.3	slightly domed	54
Co[10-2,6Cl_2P-5,15-(3NO_2P)$_2$C](PPh_3)[e]	LAMTAX	1.846	1.905	2.217	0.292	0.360	0.460	11.3	0.8	13.7	slightly saddled	55
Co[Br_8TNPC](PPh_3)[f]	QIQCUO (molecule 1)	1.917	1.869	2.207	0.300	0.389	0.446	0.1	4.6	16.9	slightly saddled	43
	QIQCUO (molecule 2)	1.832	1.879	2.239	0.261	0.341	0.433	51.1	1.7	17.5	saddled	43
Co[Br_8T*p*CF_3PC](PPh_3)	–	1.880	1.898	2.225	0.262	0.269	0.296	8.2	4.8	10.2	slightly saddled	This work
Rh[TPFPC](PPh_3)[a]	MELBUA	1.964	1.972	2.222	0.277	0.440	0.670	6.3	20.2	21.3	domed	35
Rh[TPC](PPh_3)	This work	1.947	1.971	2.210	0.279	0.400	0.563	0.8	23.0	27.6	domed	This work
Rh[T*p*OMePC](PPh_3)	This work	1.951	1.969	2.215	0.317	0.459	0.670	0.5	23.2	11.7	domed	This work

[a] TPFPC = 5,10,15-tris(pentafluorophenyl)corrole; [b] T2,4Cl_2PC = tris(2,4-dichlorophenyl)corrole; [c] T2ClPC = 5,10,15-tris(2-chlorophenyl)corrole; [d] TDFPC = tris(2,6-difluorophenyl)corrole; [e] 10-2,6Cl_2P-5,15-(3NO_2P)$_2$C = 10-(2,6-dichlorophenyl)-5,15-bis(3-nitrophenyl)corrole; [f] TNPC = 5,10,15-tris(4-nitrophenyl)corrole.

(c) UV-vis spectroscopy. By now, the optical criterion for ligand noninnonce, i.e., the sensitivity of the Soret maxima of *meso*-triarylcorrole complexes to the *para* substituents X, is well-established.5 The criterion applies well to a variety of Fe and Cu corroles, where the noninnocent character of the corrole ligand has also been established with additional spectroscopic and computational methods. Certain Ag[15] and Pt[22] corroles were also recognized as noninnocent via this criterion. On the other hand, the Soret maxima of innocent metallotriarylcorroles, including CrO, MoO, TcO, ReO, RuN, OsN, and Au corroles, are essentially invariant with respect to the *para* substituent X.[5] Against this backdrop, the optical spectra of the Group 9 metallocorroles described here (Figure 3 and Table 4) make for an interesting story.

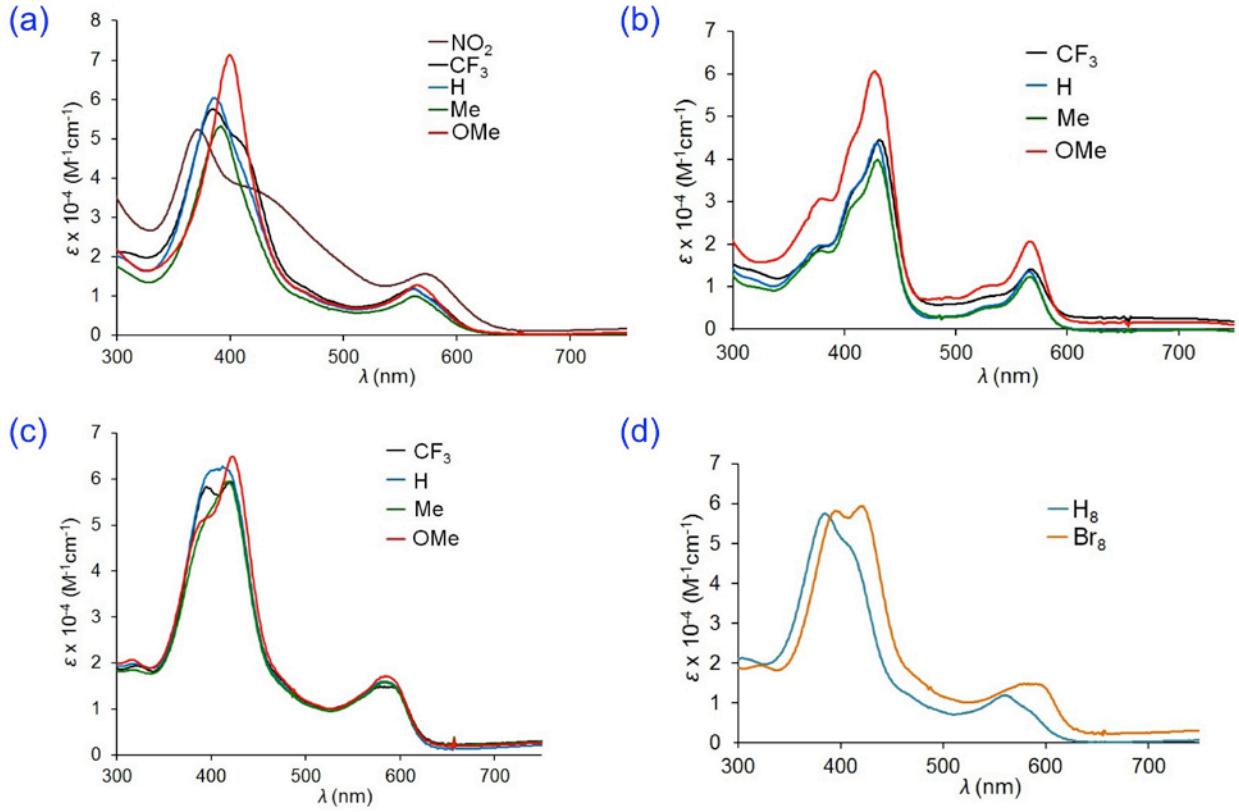

Figure 3. UV-vis spectra in dichloromethane for (a) Co[T*p*XPC](PPh$_3$), (b) Rh[T*p*XPC](PPh$_3$), (c) Co[Br$_8$T*p*XPC](PPh$_3$), and (d) Co[T*p*CF$_3$PC](PPh$_3$) and Co[Br$_8$T*p*CF$_3$PC](PPh$_3$).

Table 4. Soret λ_{max} (nm) for Co and Rh corroles studied.

Complex	*para* substituent X				
	NO_2	CF_3	H	Me	OMe
Co[T*p*XPC](PPh$_3$)	371	385	387	392	399
Co[Br$_8$T*p*XPC](PPh$_3$)	–	421	412	418	423
Rh[T*p*XPC](PPh$_3$)	–	431	429	430	427

All three series of metallocorroles investigated here exhibit split or double-humped Soret bands. In the case of Co[T*p*XPC](PPh$_3$), the higher energy peak, which corresponds to the overall band maximum, exhibits a strong sensitivity to X, shifting from 371 nm for Co[T*p*NO$_2$PC](PPh$_3$) to 399 nm for Co[T*p*OMePC](PPh$_3$). In contrast, the Soret maxima of the Rh[T*p*XPC](PPh$_3$) are clearly essentially invariant with respect to X. According to the aforementioned optical criterion, these results strongly suggest that the Co[T*p*XPC](PPh$_3$) is noninnocent, with significant Co^{II}-corrole$^{\bullet 2-}$ character, whereas the analogous Rh series is innocent, i.e., Rh^{III}-corrole^{3-}. Such a scenario is analogous to Cu and Ag[15] triarylcorroles and to FeNO and RuNO[26] triarylcorroles; in both these cases, the first-row transition metal complexes are strongly noninnocent, whereas the second-row complexes are essentially innocent.

The Soret envelope of the Co[Br$_8$T*p*XPC](PPh$_3$) series is redshifted by approximately 30 nm relative to the non-brominated Co[T*p*XPC](PPh$_3$) series. Unfortunately, the Soret bands of the brominated complexes consist of two closely spaced humps, which cannot be accurately deconvoluted. It is clear, nevertheless, that the substituent effect of X is relatively muted in the brominated series, relative to the non-brominated series. Again a parallel may be drawn to analogous behaviour of the Fe[T*p*XPC](NO) and Fe[Br$_8$T*p*XPC](NO); substituent effects on the Soret maxima of the latter series are much more muted than those in the former.[19,20] As noted before, the lack of substituent sensitivity of the Soret maxima in the brominated series most likely reflects the inability of the *meso*-aryl groups to conjugate with the corrole as a result of the steric constraints imposed by the β-bromines.[20]

(d) DFT calculations.[56,57] DFT calculations support the above interpretations. Thus, B3LYP/STO-TZP calculations yielded a broken-symmetry spin density profile for Co[TPC](PPh$_3$), consistent with a Co^{II}-corrole$^{\bullet 2-}$ description (Figure 4), as well as a surprisingly small singlet-triplet splitting of only 0.15 eV. (It may be worth adding for the uninitiated reader that these broken symmetry densities are not real and hence do not manifest themselves as peak

broadenings in the ^{1}H NMR spectra; they are nevertheless an excellent and efficient way of visualizing the antiferromagnetically coupled nature of the complexes.) In contrast, analogous calculations on Rh[TPC](PPh$_3$) yielded only a closed-shell solution as well as a larger singlet-triplet splitting of 0.69 eV, indicating an unambiguous Rh(III) ground state that is energetically well-separated from potential valence isomers. Not unexpectedly, pure functionals do not yield broken-symmetry solutions for either complex, but the same trend in singlet-triplet energy separation is observed. Thus, BP86 calculations yield singlet-triplet energy separation of 0.62 and 1.30 eV for the Co and Rh complexes, respectively. Both BP86 and B3LYP calculations revealed substantially higher metal d_{z2} character in the 'M(d_{z2}) ± corrole(a_{2u})'-based HOMO and LUMO in the Co case than in the Rh case, again indicating partial Co^{II}-corrole$^{\bullet 2-}$ for the former.

One flaw of the broken-symmetry B3LYP calculations was that they yielded an overly long Co-P distance of 2.40 Å for Co^{II}-corrole$^{\bullet 2-}$. Inclusion of Grimme's dispersion corrections in the B3LYP calculations or the use of a pure functional, with or without the dispersion correction, yielded realistic Co-P distances of ~2.25 Å. For these reasons, TDDFT simulations of the X-ray absorption spectra of Co[TPC](PPh$_3$) (and reference compounds) were carried out with the B3LYP functional employing BP86 optimized geometries, as described below.

Regardless of the functional used, the optimized geometry of Co[TPC](PPh$_3$) revealed small but unmistakeable skeletal bond length alternations in the bipyrrole half of the macrocycle, a structural feature that has recently been recognized as a characteristic of corrole$^{\bullet 2-}$ radicals.[5] Remarkably, a previously reported crystal structure of Co[TPC](PPh$_3$) also shows clear evidence of such bond length alternation (Figure 5), lending credence to partial Co^{II}-corrole$^{\bullet 2-}$ character for the complex.

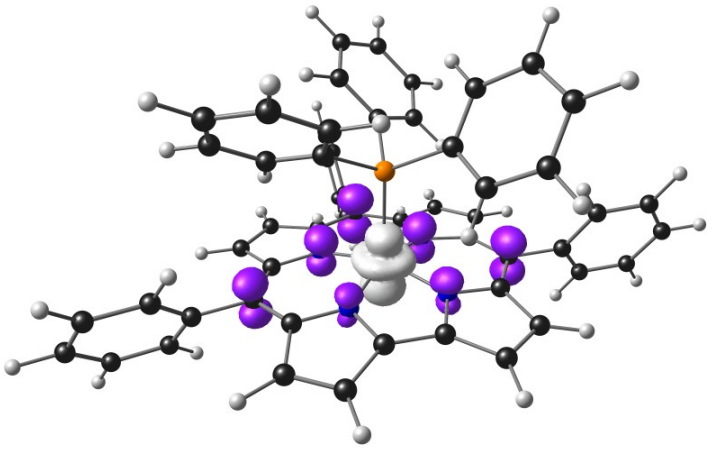

Figure 4. Broken-symmetry B3LYP/STO-TZP spin density profile (contour 0.006 e/Å^3) for Co[TPC](PPh$_3$).

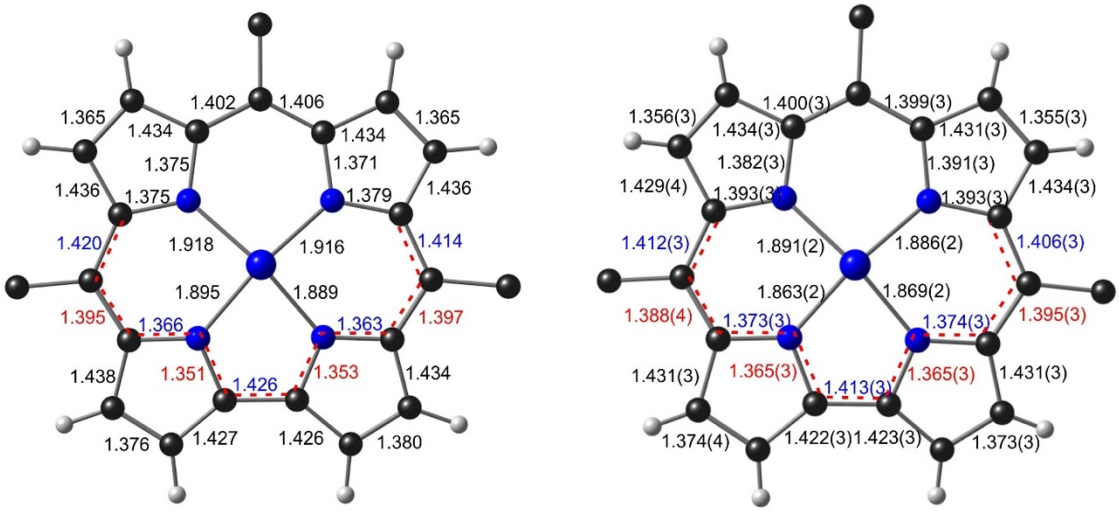

Figure 5. Skeletal bond distances for Co[TPC](PPh$_3$). Left: broken-symmetry B3LYP, right: X-ray structure (CCDC: KIMQOM).

(e) Electrochemistry.[58] Table 5 lists the redox potentials for the various complexes studied and Figure 5 depicts two representative cyclic voltammograms. All the complexes exhibit two reversible oxidations and 1-2 irreversible reductions in CH_2Cl_2 with 0.1 M TBAP. The redox potentials of the Co[Br$_8$T*p*XPC](PPh$_3$) series are generally about 450 mV upshifted relative to those of the Co[T*p*XPC](PPh$_3$) series. The Co[T*p*XPC](PPh$_3$) and Rh[T*p*XPC](PPh$_3$) series exhibit similar oxidation potentials, but significantly different reduction potentials, with the Rh complexes undergoing reduction at some 400 mV more negative potentials. The irreversibility of the reductions may be reasonably attributed to the dissociation of PPh$_3$ from the M(II) reduced state, i.e., $\{M^{II}[TpXPC]\}^-$.[59] The fact that the Co complexes are substantially easier to reduce than their Rh analogues is consistent with the greater accessibility of the Co(II) state, as revealed by the DFT calculations.

Table 5. Redox potentials (V vs. SCE) of Co/Rh-corrole-PPh$_3$ complexes studied.

Complex	E_{ox2}	E_{ox1}	$E_{red\text{-}irrev1}$	$E_{red\text{-}irrev2}$
Co[T*p*NO$_2$PC](PPh$_3$)	1.11	0.71	–0.61	–1.19[a]
Co[T*p*CF$_3$PC](PPh$_3$)	1.09	0.65	–0.82	–1.74
Co[TPC](PPh$_3$)	1.02	0.54	–0.85	–1.77
Co[T*p*MePC](PPh$_3$)	1.00	0.52	–0.89	–

Co[T*p*OMePC](PPh$_3$)	0.94	0.51	–0.91	–1.96
Co[Br$_8$T*p*CF$_3$PC](PPh$_3$)	1.28	1.08	–0.32	–1.10
Co[Br$_8$TPC](PPh$_3$)	1.21	0.99	–0.38	–1.17
Co[Br$_8$T*p*MePC](PPh$_3$)	1.18	0.97	–0.43	–1.23
Co[Br$_8$T*p*OMePC](PPh$_3$)	1.17	0.97	–0.48	–1.35
Rh[T*p*CF$_3$PC](PPh$_3$)	0.96	0.53	–1.24	---
Rh[TPC](PPh$_3$)	0.85	0.46	–1.34	---
Rh[T*p*MePC](PPh$_3$)	0.80	0.42	–1.37	---
Rh[T*p*OMePC](PPh$_3$)	0.77	0.41	–1.48	---

a The reversible reduction peak might also correspond to reduction of *p*-NO$_2$Ph groups of Co[T*p*NO$_2$PC](PPh$_3$) as observed by Kadish *et al*.[33]

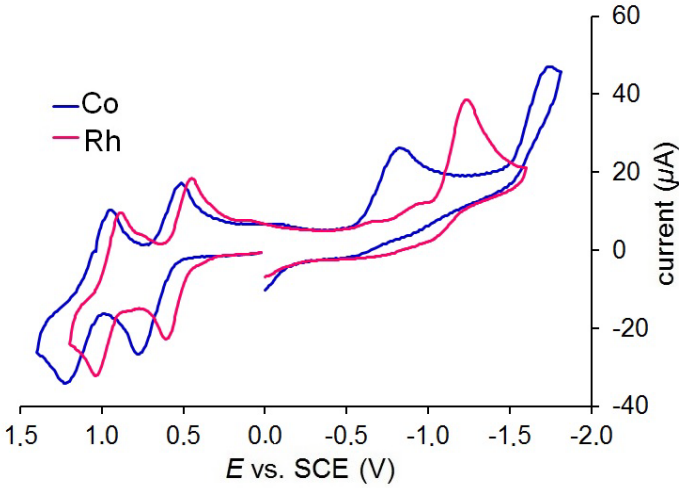

Figure 6. Cyclic voltamograms of M[T*p*CF$_3$PC](PPh$_3$) (M = Co, Rh) measured in CH_2Cl_2 with 0.1M TBAP in. Scan rate: 100 mV/s.

(f) X-ray absorption spectroscopy.[60,61,62] Cobalt K-edge XAS data were obtained for Co[TPC](PPh$_3$) and compared with those of the presumptive *bona fide* Co(III) complexes Co[TPC](py)$_2$ and Co[TPP](py)Cl[63] (TPP = tetraphenylporphyrin, Figure 7). The metal K-edge (rising edge) energy position is generally a good indicator of the charge on the absorbing metal ion.[64] Figure 7 (top inset) shows that the rising edge inflection point occurs at 7718.2, 7720.0 and 7720.4 eV for Co[TPC](PPh$_3$), Co[TPP](py)Cl and Co[TPC](py)$_2$, respectively. The sharp increase (>1.8 eV) in the rising-edge energy on going from Co[TPC](PPh$_3$) to Co[TPP](py)Cl and Co[TPC](py)$_2$ is indicative of a higher positive charge on the Co atom in the later two complexes. It is important to note, however, that the rising-edge energy is also affected by

factors other than the metal oxidation state such as multiple scattering, the metal spin state, metal-ligand distances, etc. In particular, a high-atomic number ligand tends to shift the rising edge to lower energies. Thus, the large 2.2-eV shift between Co[TPC](PPh$_3$) and Co[TPC](py)$_2$ is at least partially attributable to the presence of a heavier axial ligand in Co[TPC](PPh$_3$). For an evaluation of metal oxidation state, a better comparison is provided by Co[TPC](PPh$_3$) and Co[TPP](py)Cl, both of which have a third-period axial ligand. The 1.8 eV downshift of the rising edge in Co[TPC](PPh$_3$), relative to Co[TPP](py)Cl, thus is consistent with a lower positive charge on the Co center in the former complex.

The Co K-pre-edge region, which arises from electric-dipole–forbidden, quadrupole-allowed 1s→3d transitions, affords important information about the metal site symmetry and the ligand field strength.[65] The expanded pre-edge region (bottom inset, Figure 7) shows that pre-edge intensity weighted average energy (IWAE) values of Co[TPP](py)Cl and Co[TPC](py)$_2$ are at 7710.2 eV and 7709.9 eV, whereas the corresponding value for Co[TPC](PPh$_3$) is 7709.7 eV. These data indicate either a slight weakening of the ligand field or a lower charge on the Co center. The overall ligand field is expected to be weaker for Co[TPC](PPh$_3$), which has only five ligands relative to six in Co[TPC](py)$_2$ and Co[TPP](py)Cl, but the shift in pre-edge energy position is likely to reflect a combination of weakening ligand-field and decrease in the charge on the Co center (as indicated by the shift of the rising-edge postion to lower energies).

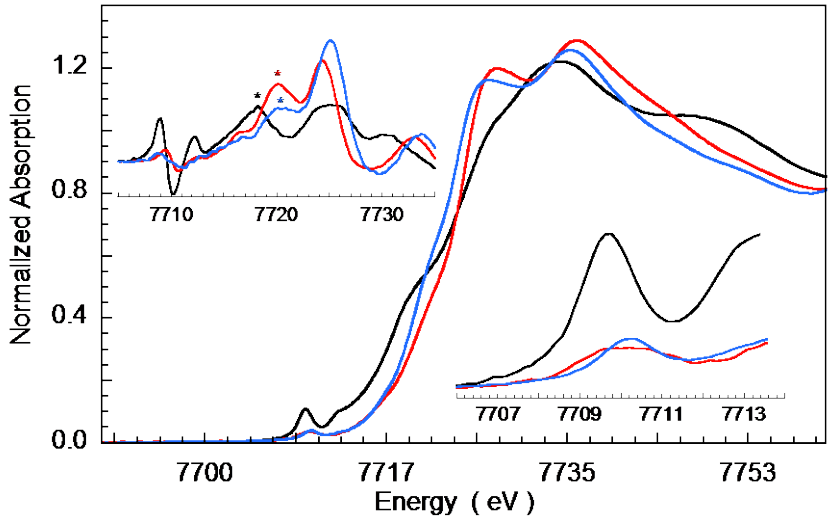

Figure 7. The normalized Co K-edge XAS spectra of Co[TPC](PPh$_3$) (black), Co[TPP](py)Cl (blue) and Co[TPC](py)$_2$ (red). The top inset depicts the first derivative spectra, where the first inflection points of the rising edge region are marked with an asterisk. The bottom inset shows the expanded pre-edge region.

(g) X-ray emission spectroscopy.[66,67] To determine the electronic structure of Co[TPC](PPh$_3$) with greater certainty, we carried out comparative Co Kβ XES measurements on Co[TPC](PPh$_3$), Co[TPC](py)$_2$ and Co[TPP](py)Cl as well as the Co(II) complex Co[TPP].[68] The spectra consist of the Co K$\beta_{1,3}$ and the Co Kβ' features, with the Co Kβ' feature gaining intensity via 3p-3d exchange interactions. These features are strongly influenced by the number of unpaired electrons at the Co center.[69] In the case of S = ½ Co(II), the unpaired 3d electron results in a small increase in the Co Kβ' intensity at ~7638 eV and a splitting of the Kβ' and the K$\beta_{1,3}$ features. This latter results in a blueshift of the K$\beta_{1,3}$ feature, as may be seen for Co[TPP] in Figure 8, thus affording a means for distinguishing between S = ½ Co(II) and S = 0 Co(III).[70]

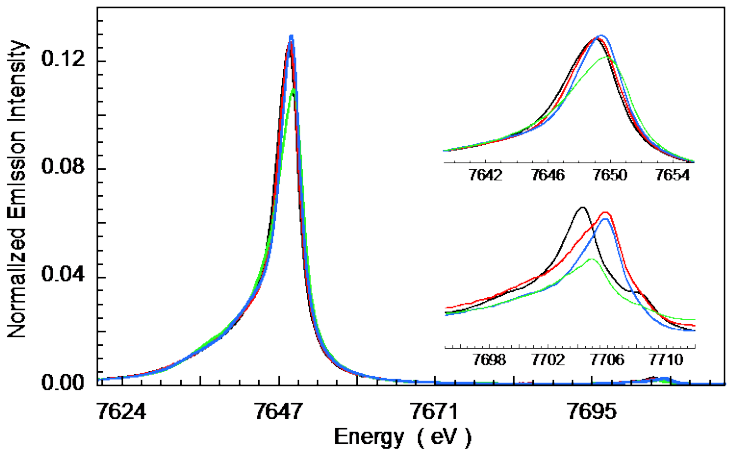

Figure 8. Normalized Co K-edge XES spectra of Co[TPC](PPh$_3$) (black), Co[TPP](py)Cl (blue), Co[TPC](py)$_2$ (red) and Co[TPP] (light green). The top inset shows the expanded K$\beta_{1,3}$ region and the bottom inset shows the expanded K$\beta_{valence}$ region.

Figure 8 shows that the Co K$\beta_{1,3}$ emission spectrum of Co[TPP] consists of a distinct, asymmetric feature with a maximum at 7649.8 eV. The asymmetry results from a low-lying Kβ' feature due to the presence of an unpaired electron at the Co center. In contrast, the complexes Co[TPC](PPh$_3$), Co[TPC](py)$_2$, and Co[TPP](py)Cl all exhibit symmetric spectra with maxima at 7648.9 eV, 7649.0, and 7649.1 eV, respectively, suggestive of a Co(III)-like ground state. A comparison of the K$\beta_{valence}$ region (bottom inset, Figure 8) reflects large differences in metal-ligand interactions among the four complexes, consistent with differences in both ligand type and coordination number.[71]

The apparent discrepancy between XAS rising-edge shift and the energy of the XES K$\beta_{1,3}$ feature can be explained on the basis of covalent interactions between the Co and the ligands and the influence of delocalization of Co 3d character into the ligand orbitals, which in turn can influence the energy position of the XES spectra. Recently, DeBeer *et al*. have demonstrated that metal-ligand covalence can have a significant influence on the splitting between the Kβ' and the K$\beta_{1,3}$ features[72], especially if it leads to significant reduction in metal character in the primarily metal d-based orbitals. This conclusion was reached on the basis of an analysis of a series of Fe complexes for which a significant redshift of the K$\beta_{1,3}$ feature was observed on going from the relatively ionic $[FeF_6]^{3-}$ to the much more covalent $[Fe(SR)_4]^{-}$ complex.

For a low-spin S = 0 Co(III) species, the Kβ'–K$\beta_{1,3}$ splitting is 0 eV, since there is no metal 3p-3d exchange interaction. For low-spin Co(II), this splitting is given by $e^2(4G_1 + 42G_3)$, where e^2 is the Stevens orbital reduction factor for the e_g orbitals and $4G_1 + 42G_3$ is the Co p-d exchange interaction energy per spin pair, which has been calculated to be 7.425 eV for a free Co(II) ion (see Table S16, ref [72]). In order to obtain the Stevens orbital reduction factors, DFT calculations were carried out on Co[TPC](PPh_3), Co[TPC]$(py)_2$, Co[TPP](py)Cl, and [Co(TPP)], as detailed in the experimental section. TDDFT calculations were also carried out to calculate the Co 1s→3d transitions and were found to yield a reasonably good simulation of the experimental Co K pre-edge XAS spectra, as shown in Figure 9.

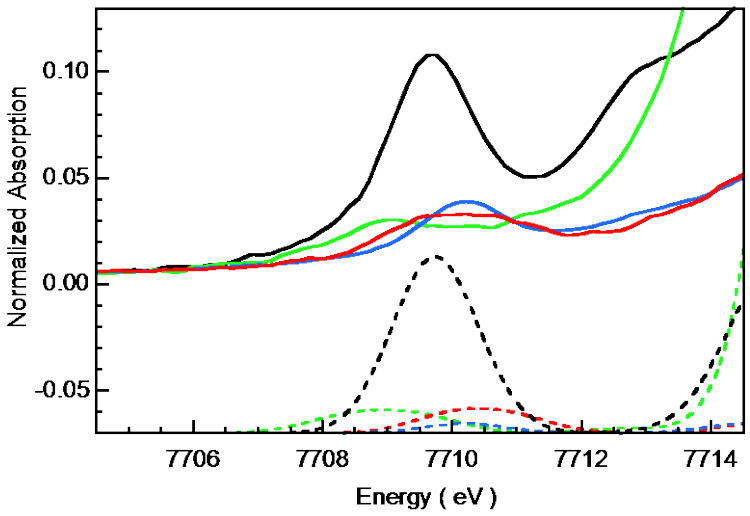

Figure 5. Comparison of TDDFT 1s→3d spectra (dotted lines) with the experimental Co K pre-edge XAS data (solid lines) for Co[TPC](PPh$_3$) (black), Co[TPP](py)Cl (blue), Co[TPC](py)$_2$ (red) and Co[TPP] (light green).

Table 6: Stevens Reduction Factors (e) Obtained from the Sum of the DFT Löwdin d Populations.

	Co[TPP]	Co[TPC](py)$_2$	Co[TPP](py)Cl	Co[TPC](PPh$_3$)
$(\alpha+\beta)3d_{z^2}$	155.8	124.3	127.5	83.2
$(\alpha+\beta)3d_{x^2-y^2}$	139.0	123.7	127.3	109.3
Total	294.8	248.0	254.7	192.5
e^2	0.54	0.38	0.41	0.23
ΔE^a (eV)	4.2	-	-	1.8

[a]ΔE is calculated by using the calculated Co p-d exchange interaction energy of 7.425 eV and is calculated for the low-spin d^7 species.

The above experimentally calibrated DFT calculations provided the Co 3d contributions to the e_g orbitals via the Löwdin method and thereby also the Stevens orbital reduction factors (Table 6). Table 6 shows that both the d_{z2} and d_{x2-y2} orbitals engage in covalent interactions with with the TPP and TPC ligands and that the interaction is especially strong for Co[TPC](PPh$_3$), leading to greater reduction in its calculated e^2 value. Like the remainder of our studies, these calculations thus also ascribe significant Co^{II}-corrole$^{\bullet 2-}$ character to the Co[TPC](PPh$_3$) complex. A hypothetical and simplistic view of Co[TPC](PPh$_3$) as purely Co^{II}-corrole$^{\bullet 2-}$ and an e^2 value of 0.23 leads to a calculated Kβ' – K$\beta_{1,3}$ splitting of 1.8 eV, which is 2.4 V lower than that of Co[TPP] and consistent with the observed blueshift of K$\beta_{1,3}$ feature of the latter complex. Since the Kβ' feature is weak for low-spin d^7 species and weakens further and crawls under the main K$\beta_{1,3}$ feature with increased metal-ligand covalence, an experimental estimation of ΔE is difficult. The ~ 0.9 eV shift between the K$\beta_{1,3}$ features of [Co(TPP)] and [Co(TPC)]PPh$_3$, however, may be viewed as reasonably consistent with theory, as it is just under half the calculated value of 2.4 eV. In other words, even if Co[TPC](PPh$_3$) were a full-fledged Co^{II}-corrole$^{\bullet 2-}$ species, its main K$\beta_{1,3}$ feature should be significantly redshifted relative to Co[TPP] because of strong metal-ligand covalence in Co[TPC](PPh$_3$). Thus, although the XES data are

not diagnostic of the Co oxidation state in Co[TPC](PPh_3), they are consistent with a highly covalent electronic structure with partial Co^{II}-$corrole^{\bullet 2-}$ character and thus also with the XAS data.

Conclusion. A multitechnique reinvestigation of cobalt-corrole-triphenylphosphine complexes has suggested that they may not be true Co(III) complexes, as long supposed, but are noninnocent with partial Co^{II}-$corrole^{\bullet 2-}$ character. Thus, the Soret maxima of Co[T*p*XPC](PPh_3) redshift markedly with increasing electron-donating character of the *meso*-aryl *para* substituent X, a key signature of corrole radical states. In contrast, the Soret maxima of Rh[T*p*XPC](PPh_3) are essentially invariant with respect to the *para* substituent X, indicating an innocent Rh^{III}-$corrole^{3-}$ description. This argument is supported by DFT B3LYP calculations on Co[TPC](PPh_3), which yielded a broken-symmetry ground-state spin density profile consistent with a Co^{II}-$corrole^{\bullet 2-}$ descriptions well as a singlet-triplet gap of only 0.15 eV. In contrast, analogous calculations on Rh[TPC](PPh_3) yielded a fully spin-paired ground state and a much higher singlet-triplet gap of 0.94 eV. Skeletal bond length alternations in the X-ray structure of Co[TPC](PPh_3) (but not the analogous Rh complexes) are also suggestive of a corrole radical. XAS measurements also revealed that the Co K rising edge of Co[TPC](PPh_3) is some 1.8 eV lower than those of the presumptive, genuine Co(III) complexes Co[TPP](py)Cl and Co[TPC]($py)_2$, consistent with a lower positive charge on the metal in Co[TPC](PPh_3). In apparent contrast to these findings, Co[TPC](PPh_3), Co[TPC]($py)_2$, and Co[TPP](py)Cl all were found to exhibit near-identical $K\beta_{1,3}$ emission maxima that are redshifted by 0.8 ± 0.1 eV relative to Co[TPP]. DFT calculations provided a rationale for this paradox in terms of a high degree of metal-ligand covalence in Co[TPC](PPh_3) relative to the other compounds. These results emphasize that spin state assignments based simply on the energy of the $K\beta_{1,3}$ feature may be erroneous, especially for highly covalent systems such as Co[TPC](PPh_3). Overall, the various lines of experimental and theoretical evidence strongly suggest that Co-corrole-PPh_3 complexes are noninnocent with partial Co^{II}-$corrole^{\bullet 2-}$ character.

Experimental section

Materials. All reagents and solvents were used as purchased unless otherwise noted. CHROMASOLV® HPLC-grade *n*-hexane and dichloromethane were used as solvents for column chromatography. Silica gel 150 (35-70 μm particle size, Davisil) was used as the stationary phase for flash chromatography and silica gel 60 preparative thin-layer

chromatographic (PLC) plates (20 x 20 cm, 0.5 mm thick, Merck) were used for final purification of the products. Triphenylphosphine was recrystallized from hot methanol and stored under nitrogen. Cobalt(II) acetate tetrahydrate, $Co(OAc)_2•4H_2O$, obtained from Merck, and bis[chloro(1,5-cyclooctadiene)rhodium(I)], $[Rh(cod)_2Cl]_2$, obtained from Sigma-Aldrich, were both used as received. Anhydrous dichloromethane for electrochemistry was prepared by distillation after pre-drying with CaH_2 and stored over 3Å molecular sieves. The starting materials, the free base corroles H_3[T*p*XPC] and free base *β*-octabromocorroles H_3[Br_8T*p*XPC] (X = CF_3, H, Me, OMe) were synthesized as previously reported.[73,74]

Instrumentation. Ultraviolet-visible spectra were recorded on an Agilent Cary 8454 UV-Visible spectrophotometer in CH_2Cl_2. Cyclic voltammetry experiments were performed with an EG&G Princeton Applied Research Model 263A potentiostat equipped with a three-electrode system consisting of a glassy carbon working electrode, a platinum wire counterelectrode, and a saturated calomel reference electrode (SCE). Tetrakis(*n*-butyl)ammonium perchlorate (Sigma-Aldrich, TBAP), recrystallized three times from absolute ethanol, vacuum-dried at 40°C for two days, and kept in a desiccator for further drying for at least two weeks, was used as the supporting electrolyte. The reference electrode was separated from bulk solution by a fritted-glass bridge filled with the solvent/supporting electrolyte mixture. All potentials were referenced to the SCE. A scan rate of 100 mV/s was used. The anhydrous dichloromethane solutions were purged with argon for at least 5 min prior to electrochemical measurements and an argon blanket was maintained over the solutions during the measurements. ^{1}H NMR spectra were recorded on a 400 MHz Bruker Avance III HD spectrometer equipped with a 5 mm BB/^{1}H (BB = ^{19}F, ^{31}P-^{15}N) SmartProbe in $CDCl_3$ and referenced to residual $CHCl_3$ (7.26 ppm), all at room temperature. High resolution Electrospray Ionization (HR-ESI) mass spectra were recorded on an LTQ Orbitrap XL spectrometer.

Synthesis of cobalt-triarylcorrole-triphenylphosphine complexes. A detailed procedure is described below for the synthesis of cobalt-tris(4-trifluoromethylphenyl)corrole-triphenylphosphine, Co[T*p*CF_3PC](PPh_3). A similar procedure was also followed for synthesis of the other Co complexes, except for details of the chromatographic purifications, which are specified separately. Cobalt corroles with electron-donating *para*-substituents (X = Me and OMe) were found to be somewhat unstable in contact with the silica gel used for column chromatography, which may have led to comparatively lower yields for these complexes.

Synthesis of Co[T*p*CF_3PC](PPh_3). To a THF solution (10 mL) of free-base tris(4-

trifluoromethylphenyl)corrole (0.025g, 0.034 mmol) in a 25-mL round-bottomed flask, was added $Co(OAc)_2.4H_2O$ (5 equiv, 0.042g, 0.17 mmol) and NaOAc (15 equiv, 0.042g, 0.51 mmol) and the resulting solution was stirred at room temperature for 5 min. Triphenylphosphine (5 equiv, 0.045g, 0.17 mmol) was then added and stirring was continued at 45 °C for 90 min, during which the color of the solution turned from green to dark red. After removal of the solvent by rotary evaporation, the dark residue obtained was chromatographed on a silica gel column (height = 12 cm) with 5:1 *n*-hexane/dichloromethane as eluent. The product eluted as an intense, dark red band, which was collected and evaporated to dryness. The resulting solid was further purified by PLC using 3:1 *n*-hexane/CH_2Cl_2 as eluent. The front red band consisted of pure Co[T*p*CF_3PC](PPh_3) (0.029g, 81%). UV-vis (CH_2Cl_2) λ_{max} [nm, ε x 10^{-4} ($M^{-1}cm^{-1}$)]: 385 (5.76), 411 (sh, 4.84), 560 (1.19). ^{1}H NMR ($CDCl_3$, 25°C) δ: 8.73 (d, J = 4.4 Hz, 2H, β-pyrrolic), 8.36 (d, J = 4.8 Hz, 2H, β-pyrrolic), 8.20 (br s, 2H, *meso*-aryl), 8.12 (s, 1H, *meso*-aryl), 8.10 (d, J = 4.8 Hz, 2H, β-pyrrolic), 8.03 (d, J = 4.4 Hz, 2H, β-pyrrolic), 7.93-7.85 (m, 5H, *meso*-aryl), 7.82 (d, J = 8.04 Hz, 1H, *meso*-aryl), 7.66 (br s, 2H, *meso*-aryl), 7.41 (d, J = 7.96 Hz, 1H, *meso*-aryl), 7.12-7.06 (m, 3H, *p*-H of PPh_3), 6.75-6.67 (m, 6H, *m*-H of PPh_3), 4.68-4.60 (m, 6H, *o*-H of PPh_3). HRMS (major isotopomer) $[M]^+$: 1048.1788 (expt), 1048.1782 (calcd). Elemental analysis found (calcd): C 66.58 (66.42), H 3.72 (3.36), N 5.19 (5.34).

Synthesis of Co[T*p*MePC](PPh_3): Silica gel column chromatography with *n*-hexane/CH_2Cl_2 (3:2) mixture as eluent afforded 0.026g (0.029 mmol, 66%) of Co[T*p*MePC](PPh_3). UV-vis (CH_2Cl_2) λ_{max} [nm, ε x 10^{-4} ($M^{-1}cm^{-1}$)]: 392 (5.33), 563 (0.99). ^{1}H NMR ($CDCl_3$, 25°C) δ: 8.57 (d, J = 4.4 Hz, 2H, β-pyrrolic), 8.33 ((d, J = 4.76 Hz, 2H, β-pyrrolic), 8.10 (d, J = 4.76 Hz, 2H, β-pyrrolic), 8.03 (d, J = 4.4 Hz, 2H, β-pyrrolic), 8.02-7.94 (broad-m, 2H, *meso*-aryl), 7.89 (d, J = 7.7 Hz, 1H, *meso*-aryl), 7.50-7.32 (m, 8H, *meso*-aryl), 7.27 (s, 1H, *meso*-aryl), 7.07-7.00 (m, 3H, *p*-H of PPh_3), 6.74-6.66 (m, 6H, *m*-H of PPh_3), 4.77-4.69 (m, 6H, *o*-H of PPh_3), 2.57 (s, 6H, 5,15-Me), 2.56 (s, 3H, 10-Me). HRMS (major isotopomer) $[M]^+$: 886.2630 (expt), 886.2630 (calcd).

Synthesis of Co[T*p*OMePC](PPh_3): Silica gel column chromatography with *n*-hexane/CH_2Cl_2 (1:1, then 1:2) as eluent afforded 0.0225g (0.024 mmol, 59%) of Co[T*p*OMePC](PPh_3). UV-vis (CH_2Cl_2) λ_{max} [nm, ε x 10^{-4} ($M^{-1}cm^{-1}$)]: 399 (7.13), 565 (1.27). ^{1}H NMR ($CDCl_3$, 25°C) δ: 8.58 (d, J = 4.4 Hz, 2H, β-pyrrolic), 8.34 (d, J = 4.76 Hz, 2H, β-pyrrolic), 8.11 (d, J = 4.76 Hz, 2H, β-pyrrolic), 8.04 (d, J = 4.4 Hz, 3H, overlapping β-pyrrolic and *meso*-aryl), 7.91 (d, J = 7.9 Hz, 1H, *meso*-aryl), 7.51 (s, 2H, *meso*-aryl), 7.29 (d, J = 7.8 Hz,

1H, *meso*-aryl), 7.20-6.99 (m, 10H, overlapping *meso*-aryl and *p*-H of PPh_3), 6.75-6.65 (m, 6H, *m*-H of PPh_3), 4.79-4.66 (m, 6H, *o*-H of PPh_3), 4.01 (s, 6H, 5,15-OMe), 4.0 (s, 3H, 10-OMe). HRMS (major isotopomer) $[M]^+$: 934.2475 (expt), 934.2478 (calcd).

Synthesis of cobalt–*β*-octabromocorrole–triphenylphosphine complexes. A detailed procedure is described below for Co[Br_8T*p*CF_3PC](PPh_3); the other *β*-octabromocorrole complexes were synthesized via a similar protocol, except for the optimum chromatographic purification, which is indicated separately for each complex. Accurate elemental analyses could not be obtained for these complexes because of decomposition on warming and rigorous drying and/or storage.

Synthesis of Co[Br_8T*p*CF_3PC](PPh_3). To a THF (10 mL) solution of free-base H_3[Br_8T*p*CF_3PC] (0.025g, 0.018 mmol) in a 50-mL round-bottomed flask, was added 5 equivalent of $Co(OAc)_2$•$4H_2O$ (0.022g, 0.09 mmol) and 5 equivalent of triphenylphosphine (0.024g, 0.09 mmol) and the solution was stirred at 50°C temperature while open to the atmosphere. The progress of the reaction was monitored by UV-Vis spectroscopy and mass spectrometry. After 30-35 min, the solvent was removed by rotary evaporation and the dark brown residue was chromatographed on a silica gel column with 4:1 *n*-hexane/dichloromethane as eluent. The product eluted as a reddish-brown band, which was collected and evaporated to dryness. Final purification was carried out with PLC using 7:3 *n*-hexane/CH_2Cl_2 as eluent. The front brownish-yellow band contained pure product Co[Br_8T*p*CF_3PC](PPh_3) (0.025g, 82%). UV-vis (CH_2Cl_2) λ_{max} [nm, ε x 10^{-4} ($M^{-1}cm^{-1}$)]: 396 (5.82), 421 (5.94), 579 (1.49). ^{1}H NMR ($CDCl_3$, 25°C): δ 7.99 (d, J = 7.9 Hz, 1H, *meso*-aryl), 7.94 (d, J = 8.0 Hz, 2H, *meso*-aryl), 7.78-7.75 (m, 6H, *meso*-aryl), 7.39 (d, J = 7.9 Hz, 1H, *meso*-aryl), 7.27-7.22 (m, 3H, *p*-H of PPh_3), 7.07 (d, J = 8.2 Hz, 2H, *meso*-aryl), 6.92-6.85 (m, 6H, *m*-H of PPh_3), 4.87-4.79 (m, 6H, *o*-H of PPh_3). HRMS (major isotopomer) $[M]^+$: 1679.4540 (expt), 1679.4554 (calcd).

Needle-shaped X-ray quality crystals were obtained by slow diffusion of MeOH vapour into a concentrated $CHCl_3$ solution of the complex over one week.

Synthesis of Co[Br_8TPC](PPh_3). Silica gel column chromatography with 3:1 *n*-hexane/CH_2Cl_2 followed by PLC with 2:1 *n*-hexane/CH_2Cl_2 as eluent afforded pure Co[Br_8TPC](PPh_3) (0.018g, 0.012 mmol, 56%). UV-vis (CH_2Cl_2) λ_{max} [nm, ε x 10^{-4} ($M^{-1}cm^{-1}$)]: 407 (6.22), 412 (6.29), 584 (1.60). ^{1}H NMR ($CDCl_3$, 25°C) δ: 7.85 (d, J = 7.7 Hz, 1H, *meso*-aryl), 7.81 (d, J = 7.6 Hz, 2H, *meso*-aryl), 7.71-7.63 (m, 3H, *meso*-aryl), 7.60-7.46 (m, 6H, *meso*-aryl), 7.33 (d, J = 7.6 Hz, 1H, *meso*-aryl), 7.25-7.18 (m, 3H, *p*-H of PPh_3), 7.01 (d, J = 7.6 Hz,

meso-aryl), 6.92-6.86 ((m, 6H, *m*-H of PPh_3), 4.95-4.87 (m, 6H, *o*-H of PPh_3). HRMS (major isotopomer) $[M]^+$: 1475.4889 (expt), 1475.4931 (calcd).

Synthesis of Co[Br_8T*p*MePC](PPh_3). Silica gel column chromatography with 3:1 *n*-hexane/CH_2Cl_2 followed by PLC with 2:1 *n*-hexane/CH_2Cl_2 as eluent afforded pure Co[Br_8T*p*MePC](PPh_3) (0.02g, 0.013 mmol, 62%). UV-vis (CH_2Cl_2) λ_{max} [nm, ε x 10^{-4} ($M^{-1}cm^{-1}$)]: 418 (5.94), 583 (1.58). ^{1}H NMR ($CDCl_3$, 25°C) δ: 7.71 (d. J = 7.6 Hz, 1H, *meso*-aryl), 7.67 (d, J = 7.6 Hz, 2H, *meso*-aryl), 7.40-7.27 (m, 6H, *meso*-aryl), 7.22-7.16 (m, 4H, *meso*-aryl and *p*-H of PPh_3 overlapping), 6.92-6.84 (m, 8H, overlapping *meso*-aryl and *m*-H of PPh_3), 4.94-4.86 (m, 6H, *o*-H of PPh_3), 2.61 (overlapping s, 9H, 5,10,15-Me protons). HRMS (major isotopomer) $[M]^+$: 1517.5397 (expt), 1517.5402 (calcd).

Synthesis of Co[Br_8T*p*OMePC](PPh_3): Silica gel column chromatography with *n*-hexane/CH_2Cl_2 (2:3, then 1:2) followed by PLC with 1:3 *n*-hexane/CH_2Cl_2 as eluent afforded pure Co[Br_8T*p*OMePC](PPh_3) (0.023g, 0.0146 mmol, 73%). UV-vis (CH_2Cl_2) λ_{max} [nm, ε x 10^{-4} ($M^{-1}cm^{-1}$)]: 393(sh, 5.14), 423 (6.49), 584 (1.72). ^{1}H NMR ($CDCl_3$, 25°C) δ: 7.74-7.65 (m, 3H, *meso*-aryl), 7.24-7.17 (m, 4H, *meso*-aryl and *p*-H of PPh_3 overlapping), 7.13-7.02 (m, 6H, *meso*-aryl), 6.93-6.85 (m, 8H, overlapping *meso*-aryl and *m*-H of PPh_3), 4.93-4.85 (m, 6H, *o*-H of PPh_3), 4.02 (overlapping s, 9H, 5,10,15-OMe). HRMS (major isotopomer) $[M]^+$: 1565.5242 (expt), 1565.5250 (calcd).

Synthesis of Co[TPC](py)$_2$. A 50 mL round-bottomed flask equipped with a magnetic stir-bar was charged with free-base triphenylcorrole (0.03 g, 0.057 mmol) dissolved in pyridine (10 mL). To this solution was added $Co(OAc)_2$•$4H_2O$ (0.142 g, 0.57 mmol). The reaction flask was then fitted with a reflux condenser and heated on an oil bath at 100°C with stirring for 25-30 min. Completion of the reaction was confirmed by UV-Vis spectroscopy and mass spectrometry. Upon cooling, the solution was rotary evaporated under high vacuum to yield a dark greenish-brown residue. The residue was redissolved in a minimum volume of dichloromethane containing a couple of drops of pyridine and was chromatographed on a silica gel column (length 10 cm) with 1:1:0.02 *n*-hexane/ dichloromethane/ pyridine as eluent. The intense green front running band was collected and identified as the title compound. Recrystallization from a mixture of 3:1 *n*-hexane/DCM with few drops of pyridine afforded the pure product (0.0326 g, 0.044 mmol, 77%). UV-vis (CH_2Cl_2) λ_{max} [nm, ε x 10^{-4} ($M^{-1}cm^{-1}$)]: 388 (10.35). UV-vis (CH_2Cl_2, 0.5% pyridine) λ_{max} [nm, ε x 10^{-4} ($M^{-1}cm^{-1}$)]: 437 (6.86), 452 (6.03), 582 (0.95), 623 (3.09). ^{1}H NMR (benzene-d_6, 25°C) δ: 9.05 (d, J = 4.3 Hz, 2H, β-pyrrolic), 8.93 (d, J = 4.6 Hz, 2H, β-

pyrrolic), 8.76-8.70 (m, 4H, *β*-pyrrolic), 8.40-8.35 (m, 4H, 5,15-*o*/*m*-aryl), 8.30-8.25 (m, 2H, 10-*o*/*m*-aryl), 7.53-7.41 (m, 9H, 5,15, & 10-*o*/*m*/*p*-aryl), 5.08 (s, 2H, *p*-H of pyridine), 4.54 (s, 4H, *m*-H of pyridine), 3.18 (broad-s, 4H, *o*-H of pyridine). HRMS (major isotopomers in presence of a drop of pyridine, M = $C_{37}H_{23}N_4Co$): $[M]^+$ (0.70) 582.1225 (expt.), 582.1249 (calcd.); $[M + py]^+$ (1.00) 661.1676 (expt.), 661. 1671 (calcd.); $[M + 2\ py]^+$ (0.30) = 740.2100 (expt), 740.2093 (calcd).

Synthesis of rhodium-corrole-triphenylphosphine complexes. A detailed procedure is described below for the synthesis of rhodium-tris(4-trifluoromethylphenyl)corrole-triphenylphosphine complex, Rh[T*p*CF_3PC](PPh_3). A similar procedure was also followed for synthesis of the other Rh complexes, except for the optimum methods for chromatographic purifications, which are specified separately.

Synthesis of Rh[T*p*CF_3PC](PPh_3). To a solution of free base tris(4-trifluoromethylphenyl)corrole (0.010g, 0.014 mmol) in 2:1 dichloromethane/ethanol (15 mL) in a 50ml round bottomed flask, was added sequentially $[Rh(cod)_2Cl]_2$ (0.0103g, 0.021 mmol, 1.5 equiv), NaOAc (0.017g, 0.21 mmol, 15 equiv), and triphenyl phosphine (0.004g, 0.014 mmol, 1 equiv) and the flask was stirred at room temperature for about 30-35 min while open to the atmosphere. Completion of the reaction was confirmed by UV-vis spectroscopy and mass spectrometry. The solvent was then removed by rotary evaporation and the dark residue was chromatographed on a silica gel column with 9:1 *n*-hexane/CH_2Cl_2 as eluent. A dark red band that emerged second from the column was identified as containing Rh[T*p*CF_3PC](PPh_3). Recrystallization from hexane afforded the pure product (0.008g, 0.007 mmol, 52%). UV-vis (CH_2Cl_2) λ_{max} [nm, ε x 10^{-4} ($M^{-1}cm^{-1}$)]: 380(sh)(1.93), 431 (4.45), 568 (1.39). ^{1}H NMR ($CDCl_3$, 25°C) δ: 8.78 (d, J = 4.3 Hz, 2H, *β*-pyrrolic), 8.59 (d, J = 4.7 Hz, 2H, *β*-pyrrolic), 8.25 (d, J = 4.7 Hz, 2H, *β*-pyrrolic), 8.12 (d, J = 4.3 Hz, 2H, *β*-pyrrolic), 8.11-7.86 (m, 11H, *meso*-aryl), 7.51 (d, J = 7.8 Hz, 1H, *meso*-aryl), 7.08 (t, J = 7.3 Hz, 3H, *p*-H of PPh_3), 6.74-6.68 (m, 6H, *m*-H of PPh_3), 4.42 (dd, J=12.4, 7.8 Hz, 6H, *o*-H of PPh_3). HRMS (major isotopomer) $[M]^+$: 1092.1498 (expt), 1092.1505 (calcd). Elemental analysis found (calcd): C 63.57 (63.75), H 3.75 (3.23), N 5.04 (5.13).

Synthesis of Rh[TPC](PPh_3): Silica gel column chromatography with 9:1 *n*-hexane/ethyl acetate as eluent followed by recrystallization from 4: 1 *n*-hexane/CH_2Cl_2 afforded the pure product (0.008 g, 0.009 mmol, 48%). UV-vis (CH_2Cl_2) λ_{max} [nm, ε x 10^{-4} ($M^{-1}cm^{-1}$)]: 381 (1.97), 429 (4.38), 566 (1.35). ^{1}H NMR ($CDCl_3$, 25°C) δ: 8.71 (d, J = 4.3 Hz, 2H, *β*-

pyrrolic), 8.58 (d, *J* = 4.7 Hz, 2H, *β*-pyrrolic), 8.25 (d, *J* = 4.7 Hz, 2H, *β*-pyrrolic), 8.13 (d, *J* = 4.3 Hz, 2H, *β*-pyrrolic), 7.97(br s, 5H, *meso*-aryl), 7.76-7.57 (m, 9H, *meso*-aryl), 7.47 (d, *J* = 6.9 Hz, 1H, *meso*-aryl), 7.04 (t, *J* = 7.6 Hz, 3H, *p*-H of PPh_3), 6.77-6.66 (m, 6H, *m*-H of PPh_3), 4.47 (dd, 6H, *J*=12.3, 7.8 Hz, 6H, *o*-H of PPh_3). HRMS (major isotopomer) $[M]^+$: 888.1866 (expt), 888.1884 (calcd). Elemental analysis found (calcd): C 73.71 (74.32), H 4.53 (4.31), N 6.33 (6.30).

X-ray quality crystals were obtained by slow evaporation of a concentrated solution of the complex in 3:1 *n*-hexane/CH_2Cl_2.

Synthesis of Rh[T*p*MePC](PPh$_3$): Silica gel column chromatography with 9:1 *n*-hexane/ethyl acetate as eluent followed by recrystallization from 4:1 *n*-hexane/CH_2Cl_2 afforded the pure product (0.009 g, 0.0097 mmol, 54%). UV-vis (CH_2Cl_2) λ_{max} [nm, ε x 10^{-4} ($M^{-1}cm^{-1}$)]: 381 (1.84), 430 (3.99), 567 (1.23). ^{1}H NMR ($CDCl_3$, 25°C): δ 8.68 (d, *J* = 4.3 Hz, 2H, *β*-pyrrolic), 8.58 (d, *J* = 4.7 Hz, 2H, *β*-pyrrolic), 8.25 (d, *J* = 4.7 Hz, 2H, *β*-pyrrolic), 8.13 (d, *J* = 4.3 Hz, 2H, *β*-pyrrolic), 7.92-7.80 (m, 5H, *meso*-aryl), 7.56-7.33 (m, 7H, *meso*-aryl), 7.02 (t, *J* = 7.4 Hz, 3H, *p*-H of PPh_3), 6.72-6.64 (m, 6H, *m*-H of PPh_3), 4.46 (dd, 6H, *J* =12.2, 8.0 Hz, 6H, *o*-H of PPh_3), 2.65 (s, 6H, 5,15-Me), 2.62 (s, 3H, 10-Me). HRMS (major isotopomer) $[M]^+$: 930.2374 (expt), 930.2353 (calcd). Elemental analysis found (calcd): C 73.73 (74.84), 5.49 (4.76), 5.50 (6.02).

Synthesis of Rh[T*p*OMePC](PPh$_3$). Silica gel column chromatography with *n*-hexane/ethyl acetate (4:1 decreasing to 1:1) mixture as eluent followed by recrystallization from 3:1 *n*-hexane/CH_2Cl_2 afforded 0.0085g (0.0087 mmol) of pure Rh[T*p*OMePC](PPh_3). Yield = 54%. UV-vis (CH_2Cl_2) λ_{max} [nm, ε x 10^{-4} ($M^{-1}cm^{-1}$)]: 380 (3.1), 427 (6.06), 567 (2.06). ^{1}H NMR ($CDCl_3$, 25°C): δ 8.68 (d, *J* = 4.3 Hz, 2H, *β*-pyrrolic), 8.58 (d, *J* = 4.7 Hz, 2H, *β*-pyrrolic), 8.25 (d, *J* = 4.7 Hz, 2H, *β*-pyrrolic), 8.11 (d, *J* = 4.3 Hz, 2H, *β*-pyrrolic), 7.87 (broad-d, *J* = 8.0 Hz, 5H, *meso*-aryl), 7.35 (d, *J* = 8.1 Hz, 1H, *meso*-aryl), 7.29-7.12 (m, 6H, *meso*-aryl), 7.02 (t, *J* = 7.2 Hz, 3H, *p*-H of PPh_3), 6.71-6.64 (m, 6H, *m*-H of PPh_3), 4.45 (dd, *J* = 12.3 Hz, 7.8 Hz, 6H, *o*-H of PPh_3), 4.05 (s, 6H, 5,15-alkyl proton), 4.03 (s, 3H, 10-alkyl proton). HRMS (ESI^+,major isotopomer): $[M]^+$ = 978.2197 (expt.), 978.2201 (calcd.). Elemental analysis found (calcd): C 69.07 (71.17), 4.83 (4.53), 5.61 (5.72).

X-ray quality crystals were obtained by slow diffusion of *n*-heptane vapour into a concentrated benzene solution of the complex over one week.

Crystal Structure Determination. X-ray diffraction data were collected on beamline 11.3.1 at the Advanced Light Source. Single crystals were selected and coated in protective oil, before being transferred onto a MiTeGen kapton micromount and transferred to a Bruker D8 diffractometer fitted with a PHOTON100 CMOS detector operating in shutterless mode. The samples were cooled to 100(2) K in a nitrogen stream provided by an Oxford Cryostream 800 Plus. Diffraction data were collected using a synchrotron radiation monochromated using a silicon (111) crystal to $\lambda = 0.7749(1)$ Å. The structures were solved using dual space methods using SHELXT[75] and refined on F^2 using SHELXL-2014[76] (G. M. Sheldrick, *Acta Cryst. C, Struct. Chem.*, 2015, **71**, 3-8.). All non-hydrogen atoms were refined anisotropically. Hydrogen atoms have been included at their geometrically estimated positions. One bromine atom in Co[Br_8T*p*CF_3PC](PPh_3) is disordered and has been modelled over two sites with complementary occupancies. The two sites have been constrained to have equal U_{ij} values.

Computational methods. Ground state DFT calculations were carried with the ADF program system,[77] the B3LYP exchange-correlation functional (20% Hartree-Fock exchange),[78,79] ZORA STO-TZP basis sets, and both with and without the Grimme's D3 dispersion correction.[80] DFT calculations related to the XAS/XES measurements were carried out with the ORCA 3.0.3 program using the BP86 optimized geometries followed by single-point spin-unrestricted B3LYP calculations allowing for broken-symmetry solutions. For the latter calculations, we used the core-properties basis sets as implemented in ORCA, viz. CP(PPP) for Co and the Ahlrichs's TZVP basis set for all other atoms. These calculations also employed the conductor-like screening model (COSMO) with a dielectric constant of 3.9 as well as appropriately fine grids and tight SCF convergence criteria. For TDDFT calculations of Co K pre-edge transitions, we set the number of roots at 40, MaxDim at 400, selected "doQuad True", and did not calculate triplets. The TDDFT calculations were carried out over the entire valence manifold and for both spin-up (OrbWin=0) and spin-down(OrbWin=1) transitions. The calculated transition energies were broadened with half-widths of 1.7 eV to account for core-hole lifetime and instrument broadening and linearly upshifted by 164.5 eV for comparison with the experimental spectra.

X-ray absorption data collection and analysis. The Co K-edge X-ray absorption spectra of Co[TPP], Co[TPP)(py)Cl, Co[TPC](py)$_2$ and Co[TPC](PPh_3) were collected at the Stanford Synchrotron Radiation Lightsource under standard ring conditions of 3 GeV and ~500 mA on the unfocused 20-pole 2 T wiggler side-station 7-3, equipped with a Si(220) double

crystal monochromator for energy selection. The M_0 mirror was not employed and the monochromator was detuned by ~55% to eliminate contributions from higher harmonics. All complexes were measured as solids ground to a homogenous powder in a BN matrix. The sample was placed in Al spacers and wrapped in Kapton tape. During data collection, the samples were maintained at a constant temperature of ~10-15 K using an Oxford liquid He cryostat. Co K-edge EXAFS data were measured to k = 15 $Å^{-1}$ (transmission mode) using ion-chamber detectors. Internal energy calibration was accomplished by simultaneous measurement of the absorption of a Co-foil placed between the second and third ionization chambers situated after the sample. The data was calibrated to the first inflection point of the Co foil (7709.5 eV). The energy calibration, background correction, data averaging and normalization was accomplished with ATHENA, which is part of the Demeter software package version 0.9.24.[81] The pre-edge region of the data sets were fit using Peak-Fit (SigmaPlot).

X-ray emission data collection and analysis. Co K-edge XES spectra were measured on the 54-pole, 1-Tesla wiggler beamline 6–2. A liquid-nitrogen–cooled double crystal Si(111) monochromator was used to set the incident energy at 9 keV. Vertical and horizontal focusing mirrors were used to achieve a beam size of 150 x 400 mm. Energy calibration was achieved with a Co foil. The first inflection point of the foil spectrum was set at 7709.5 eV. Kβ X-ray emission spectra were measured using the 533 reflection of five spherically bent Si crystal analyzers in combination with a silicon drift detector aligned in a Rowland geometry, as previously described.[82] The overall energy bandwidth of the X-ray emission spectrometer was ~1.5 eV. The data were normalized with respect to the Kα line intensity. The K$\beta_{1,3}$ and the K$\beta_{valence}$ spectra were recorded separately using different regions with significant overlap between the two regions for accurate merging of the two datasets. A higher number of K$\beta_{valence}$ scans were required to achieve similar signal quality.

Acknowledgement. This work was supported by grants 231086 and 262229 of the Research Council of Norway (AG), the SSRL Structural Molecular Biology (SMB) resource (RS), the Advanced Light Source, Berkeley, California (LJM, KJG), and the National Research Fund of the Republic of South Africa (JC). The SSRL SMB resource is supported by the NIH National Institute of General Medical Sciences (NIGMS) through a Biomedical Technology Research Resource P41 grant (P41GM103393) and by the DOE Office of Biological and Environmental Research. The Advanced Light Source is supported by the Director, Office of Science, Office of Basic Energy Sciences of the U.S. Department of Energy under Contract No.

DE-AC02-05CH11231. LJG was supported by a postdoctoral fellowship from Stanford University.

References

[1] Jørgensen, C. K. Differences between the Four Halide Ligands, and discussion remarks on Trigonal-Bipyramidal Complexes, on Oxidation States, and on Diagonal Elements of One-Electron Energy. *Coord. Chem. Rev.* **1966**, *1*, 164-178.

[2] For a set of *Inorganic Chemistry* Forum articles, see: Chirik, P. J. Preface: Forum on Redox-Active Ligands. *Inorg. Chem.* **2011**, *50*, 9737-9740.

[3] Kaim, W. Manifestations of Noninnocent Ligand Behavior. *Inorg. Chem*. **2011**, *50*, 9752–9765.

[4] Lyaskovskyy, V.; de Bruin, B. Redox Non-Innocent Ligands: Versatile New Tools to Control Catalytic Reactions. *ACS Catal.* **2012**, *2*, 270–279.

[5] Ghosh, A. Electronic Structure of Corrole Derivatives: Insights from Molecular Structures, Spectroscopy, Electrochemistry, and Quantum Chemical Calculations. *Chem. Rev.* **2017**, *117*, 3798-3881.

[6] Wasbotten, I. H.; Wondimagegn, T.; Ghosh, A. Electronic Absorption, Resonance Raman, and Electrochemical Studies of Planar and Saddled Copper(III) *Meso*-Triarylcorroles. Highly Substituent-Sensitive Soret Bands as a Distinctive Feature of High-Valent Transition Metal Corroles. *J. Am. Chem. Soc.* **2002,** *124*, 8104-8116.

[7] Steene, E.; Dey, A.; Ghosh, A. *β*-Octafluorocorroles. *J. Am. Chem. Soc.* **2003,** *125*, 16300-16309.

[8] Brückner, C.; Briñas, R. P.; Bauer, J. A. K. X-ray Structure and Variable Temperature NMR Spectra of [*meso*-Triarylcorrolato]copper(III). *Inorg. Chem.* **2003**, *42*, 4495–4497.

[9] Bröring, M.; Bregier, F.; Tejero E. C.; Hell, C.; Holthausen M. C. Revisiting the Electronic Ground State of Copper Corroles. *Angew. Chem., Int. Ed.* **2007**, *46*, 445–448.

[10] Thomas, K. E.; Wasbotten, I. H.; Ghosh, A. Copper *β*-Octakis(Trifluoromethyl)Corroles: New Paradigms for Ligand Substituent Effects in Transition Metal Complexes. *Inorg. Chem.* **2008,** *47*, 10469-10478.

([11]) Alemayehu, A. B.; Conradie, J.; Ghosh, A. A First TDDFT Study of Metallocorrole Electronic Spectra: Copper *meso*-Triarylcorroles Exhibit *Hyper* Spectra. *Eur. J. Inorg. Chem.* **2011**, *12*, 1857–1864.

([12]) Alemayehu, A. B.; Hansen, L. K.; Ghosh, A. Nonplanar, Noninnocent, and Chiral: A Strongly Saddled Metallocorrole. *Inorg. Chem.* **2010,** *49*, 7608-7610.

([13]) Thomas, K. E.; Conradie, J.; Hansen, L. K.; Ghosh, A. A Metallocorrole with Orthogonal Pyrrole Rings. *Eur. J. Inorg. Chem.* **2011**, 1865–1870.

([14]) Berg, S.; Thomas, K. E.; Beavers, C. M.; Ghosh, A. Undecaphenylcorroles. *Inorg. Chem.* **2012,** *51*, 9911-9916.

([15]) Thomas, K. E.; Vazquez-Lima, H.; Fang, Y.; Song, Y.; Gagnon, K. J.; Beavers, C. M.; Kadish, K. M.; Ghosh, A. Ligand Noninnocence in Coinage Metal Corroles: A Silver Knife-Edge. *Chem. - Eur. J.* **2015,** *21*, 16839-16847.

([16]) Steene, E.; Wondimagegn, T.; Ghosh, A. Electrochemical and Electronic Absorption Spectroscopic Studies of Substituent Effects in Iron(IV) and Manganese(IV) Corroles. Do the Compounds Feature High-Valent Metal Centers or Noninnocent Corrole Ligands? Implications for Peroxidase Compound I and II Intermediates. *J. Phys. Chem. B* **2001,** *105*, 11406-11413. Addition/correction: *J. Phys. Chem. B* **2002**, *106*, 5312-5312.

([17]) Zakharieva, O.; Schünemann, V.; Gerdan, M.; Licoccia, S.; Cai, S.; Walker, F. A.; Trautwein, A. X. Is the Corrolate Macrocycle Innocent or Noninnocent? Magnetic Susceptibility, Mössbauer, ^{1}H NMR, and DFT Investigations of Chloro- and Phenyliron Corrolates. *J. Am. Chem. Soc* **2002**, *124*, 6636-6648.

([18]) Walker, F. A.; Licoccia, S.; Paolesse, R. Iron Corrolates: Unambiguous Chloroiron(III) (Corrolate)$^{2-\cdot}$ π-Cation Radicals. *J. Inorg. Biochem.* **2006,** *100*, 810-837.

([19]) Vazquez-Lima, H.; Norheim, H. K.; Einrem, R. F.; Ghosh, A. Cryptic Noninnocence: FeNO Corroles in a New Light. *Dalton Trans*. **2015**, *44*, 10146-10151.

([20]) Norheim, H.-K.; Capar, J.; Einrem, R. F.; Gagnon, K. J.; Beavers, C. M.; Vazquez-Lima, H.; Ghosh, A. Ligand Noninnocence in FeNO Corroles: Insights from β-Octabromocorrole Complexes. *Dalton Trans.* **2016,** *45*, 681-689.

([21]) Ganguly, S.;Vazquez-Lima, H.; Ghosh, A. Wolves in Sheep's Clothing: μ-Oxo-Diiron Corroles Revisited. *Chem. Eur. J.* **2016**, 22, 10336-10340.

[22] Alemayehu, A. B.; Vazquez-Lima, H.; Beavers, C. M.; Gagnon, K. J.; Bendix, J.; Ghosh, A. Platinum Corroles. *Chem. Comm*. **2014**, *50*, 11093-11096.

[23] Johansen, I.; Norheim, H.-K.; Larsen, S.; Alemayehu, A. B.; Conradie, J.; Ghosh, A. Substituent Effects on Metallocorrole Spectra: Insights from Chromium-Oxo and Molybdenum-Oxo Triarylcorroles. *J. Porphyrins Phthalocyanines* **2011**, *15*, 1335-1344.

[24] Einrem, R. F.; Braband, H.; Fox, T.; Vazquez-Lima, H.; Alberto, R.; Ghosh, A. Synthesis and molecular structure of ^{99}Tc Corroles. *Chem. Eur. J.* **2016**, *22*, 18747–18751.

[25] Einrem, R. F.; Gagnon, K. J.; Alemayehu, A. B.; Ghosh, A. Metal-Ligand Misfits: Facile Access to Rhenium-Oxo Corroles by Oxidative Metalation. *Chem. Eur. J.* **2016,** *22*, 517-520.

[26] Alemayehu, A. B.; Vazquez-Lima, H. Gagnon, K. J.; Ghosh, A. Stepwise Deoxygenation of Nitrite as a Route to Two Families of Ruthenium Corroles: Group 8 Periodic Trends and Relativistic Effects. *Inorg. Chem.* **2017***, 56*, 5285–5294.

[27] Alemayehu, A. B.; Gagnon, K. J.; Terner, J.; Ghosh, A. Oxidative Metalation as a Route to Size-Mismatched Macrocyclic Complexes: Osmium Corroles. *Angew. Chem. Int. Ed*. **2014**, *53*, 14411-14414.

[28] Alemayehu, A. B.; Ghosh, A. Gold Corroles. *J. Porphyrins Phthalocyanines* **2011**, *15*, 106-110.

[29] Rabinovitch, E.; Goldberg, I.; Gross, Z. Gold(I) and Gold(III) Corroles. *Chem. Eur. J.* **2011**, *17*, 12294–12301.

[30] Thomas, K. E.; Alemayehu, A. B.; Conradie, J.; Beavers, C.; Ghosh, A. Synthesis and Molecular Structure of Gold Triarylcorroles. *Inorg. Chem.* **2011**, *50*, 12844–12851.

[31] Mahammed A.; Giladi I.; Goldberg I.; Gross Z. Synthesis and Structural Characterization of a Novel Covalently-Bound Corrole Dimer. *Chem. Eur. J.* , **2001**, *7*, 4259-4265.

[32] Huang, S.; Fang, Y.; Lü, A.; Lu, G.; Ou, Z.; Kadish, K. M. Synthesis, Characterization and Solvent/Structural Effects on Spectral and Redox Properties of Cobalt Triphenylcorroles in Nonaqueous Media. *J. Porphyrins Phthalocyanines* **2012**, *16*, 958-967.

[33] Li, B.; Ou, Z.; Meng, D.; Tang, J.; Fang, Y.; Liu, R.; Kadish, K. M. Cobalt triarylcorroles containing One, Two or Three Nitro Groups. Effect of NO_2 Substitution on Electrochemical Properties and Catalytic Activity for Reduction of Molecular Oxygen in Acid Media. *J Inorg. Biochem*. **2014**, *136*, 130–139.

[34] Simkhovich, L.; Mahammed, A.; Goldberg, I.; Gross, Z. Synthesis and Characterization of Germanium, Tin, Phosphorus, Iron, and Rhodium Complexes of Tris(pentafluorophenyl)corrole, and the Utilization of the Iron and Rhodium Corroles as Cyclopropanation Catalysts. *Chem. Eur. J*. **2001**, *7*, 1041-1055.

[35] Simkhovich, L.; Galili, N.; Saltsman, I.; Goldberg, I.; Gross, Z. Coordination Chemistry of the Novel 5,10,15-Tris(pentafluorophenyl)corrole: Synthesis, Spectroscopy, and Structural

Characterization of Its Cobalt(III), Rhodium(III), and Iron(IV) Complexes. *Inorg. Chem.* **2000,** *39*, 2704-2705.

[36] Dogutan, D. K.; McGuire, R., Jr.; Nocera, D. G. Electocatalytic Water Oxidation by Cobalt(III) Hangman *β*-Octafluoro Corroles. *J. Am. Chem. Soc*. **2011**, *133*, 9178–9180.

[37] Mondal, B.; Sengupta, K.; Rana, A.; Mahammed, A.; Botoshansky, M.; Dey, S. G.; Gross, Z.; Dey, A. Cobalt Corrole Catalyst for Efficient Hydrogen Evolution Reaction from H_2O under Ambient Conditions: Reactivity, Spectroscopy, and Density Functional Theory Calculations*Inorg. Chem*. **2013**, *52*, 3381–3387

[38] Mahammed, A.; Mondal, B.; Rana, A.; Dey, A. Gross, Z. The Cobalt Corrole Catalyzed Hydrogen Evolution Reaction: Surprising Electronic Effects and characterization of key reaction intermediates. *Chem. Comm.* **2014**, *50*, 2725-2727.

[39] Yang, S.; Wo, Y.; Meyerhoff, M. E. Polymeric Optical Sensors for Selective and Sensitive Nitrite Detection Using Cobalt(III) Corrole and Rhodium(III) Porphyrin as Ionophores. *Anal. Chim. Acta* **2014**, *843*, 89–96.

[40] Guilard, R.; Gros, C. P.; Bolze, F.; Jerome, F.; Ou, Z.; Shao, J.; Fischer, J.; Weiss, R.; Kadish, K. Alkyl and Aryl Substituted Corroles. 1. Synthesis and Characterization of Free Base and Cobalt Containing Derivatives. X-ray Structure of $(Me_4Ph_5Cor)Co(py)_2$. *Inorg. Chem.* **2001,** *40,* 4845-4855.

[41] Barbe, J.-M.; Canard, G.; Brandes, S.; Jerome, F.; Dubois, G.; Guilard, R. Metallocorroles as Sensing Components for Gas Sensors: Remarkable Affinity and Selectivity of Cobalt(III) corroles for CO vs. O_2 and N_2. *Dalton Trans.* **2004**, 1208-1214.

[42] Vazquez-Lima, H.; Conradie, J.; Ghosh, A. Metallocorrole Interactions with Carbon Monoxide, Nitric Oxide, and Nitroxyl – A DFT Study of Low-Energy Bound States. *Inorg. Chem.* **2016**, *55*, 8248–8250.

[43] Paolesse, R.; Nardis, S.; Sagone, F.; Khoury, R. G. Synthesis and Functionalization of *meso*-Aryl-Substituted Corroles. *J. Org. Chem.* **2001**, *66*, 550-556.

[44] Paolesse, R.; Mini, S.; Sagone, F.; Boschi, T.; Jaquinod, L.; J. Nurco, D.; M. Smith, K. 5,10,15-Triphenylcorrole: A Product from a Modified Rothemund reaction. *Chem. Commun.* **1999**, 1307-1308.

[45] Simkhovich, L.; Goldberg, I.; Gross, Z. Easy Preparation of Cobalt Corrole and Hexaphyrin and Isolation of New Oligopyrroles in the Solvent-Free Condensation of Pyrrole with Pentafluorobenzaldehyde. *Org. Lett.* **2003**, *5*, 1241-1244.

[46] Thomas, K. E.; Conradie, J.; Hansen, L. K.; Ghosh, A. Corroles Cannot Ruffle. *Inorg. Chem.* **2011**, *50*, 3247-3251.

[47] Palmer, J. H.; Mahammed, A.; Lancaster, K. M.; Gross, Z.; Gray, H. B. Structures and Reactivity Patterns of Group 9 Metallocorroles. *Inorg. Chem.* **2009**, *48*, 9308-9315.

[48] Collman, J. P.; Wang, H. J. H.; Decreau, R. A.; Eberspacher, T. A.; Sunderland, C. J. Synthesis and Characterization of Rh^{III} corroles: Unusual Reactivity Patterns Observed during Metalation Reactions. *Chem. Commun.* **2005**, 2497-2499.

[49] Thomas, K. E.; Alemayehu, A. B.; Conradie, J.; Beavers, C. M.; Ghosh, A. The Structural Chemistry of Metallocorroles: Combined X-ray Crystallography and Quantum Chemistry Studies Afford Unique Insights. *Acc. Chem. Res.* **2012**, *45*, 1203-1214.

[50] Pyykkö, P.; Atsumi, M. Molecular Single-Bond Covalent Radii for Elements 1–118. *Chem. Eur. J.* **2009**, *15*, 186-197.

[51] Shannon, R. D. Revised Effective Ionic Radii and Systematic Studies of Interatomic Distances in Halides and Chalcogenides. *Acta Cryst. Sec. A* **1976**, *32*, 751–767.

[52] Dronskowski, R. *Computational Chemistry of Solid State Materials.* Wiley-VCH, **2007**, pp 1-294.

[53] Tang, J.; Ou, Z.; Ye, L.; Yuan, M.; Fang, Y.; Xue, Z.; Kadish, K. M. Meso-dichlorophenyl Substituted Co(III) corrole: A Selective Electrocatalyst for the Two-Electron Reduction of Dioxygen in Acid Media, X-ray Crystal Structure Analysis and Electrochemistry. *J. Porphyrins Phthalocyanines* **2014**, *18*, 891-898.

[54] Rui, G.; Zhong-Ping, O.; Li-Na, Y.; Wen-Hao, H.; Zhao-Li, X.; Ji-Jun, T.; Yuan-Yuan, F. Cobalt Triarylcorroles with Sterically Hindered Halogenated Phenyl Rings: Synthesis, Crystal Structure and Catalytic Activity for Electroreduction of Dioxygen. *Chinese J. Struct. Chem.* **2016**, *35*, 1754-1763.

[55] Niu, Y.; Li, M.; Zhang, Q.; Zhu, W.; Mack, J.; Fomo, G.; Nyokong, T.; Liang, X. Halogen Substituted A_2B type Co(III)Triarylcorroles: Synthesis, Electronic Structure and Two Step Modulation of Electrocatalyzed Hydrogen Evolution Reactions. *Dyes and Pigments* **2017**, *142*, 416-428.

[56] Ghosh, A.; Wondimagegn, T.; Parusel, A. B. J. Electronic Structure of Gallium, Copper, and Nickel Complexes of Corrole. High-Valent Transition Metal Centers Versus Noninnocent Ligands. *J. Am. Chem. Soc.* **2000**, *122*, 5100-5104.

[57] Ghosh, A.; Steene, E. High-Valent Transition Metal Centers and Noninnocent Ligands in Metalloporphyrins and Related Molecules: A Broad Overview Based on Quantum Chemical Calculations. *J. Biol. Inorg. Chem.* **2001,** *6*, 739-752.

[58] Fang, Y.; Ou, Z.; Kadish, K. M. Electrochemistry of Corroles in Nonaqueous Media. *Chem. Rev.* **2017**, *117*, 3377-3419.

[59] Kadish, K. M.; Koh, W.; Tagliatesta, P.; Sazou, D.; Paolesse, R.; Licoccia, S.; Boschi, T. Electrochemistry of rhodium and cobalt corroles. Characterization of (OMC)Rh(PPh_3) and (OMC)Co(PPh_3) where OMC is the Trianion of 2,3,7,8,12,13,17,18-Octamethylcorrole. *Inorg. Chem.* **1992**, *31*, 2305-2313.

[60] Palmer, J. H.; Lancaster, K. M. Molecular Redox: Revisiting the Electronic Structures of the Group 9 Metallocorroles. *Inorg. Chem.* **2012**, *51*, 12473-12482.

[61] Sarangi, R.; Giles, L. J.; Thomas, K. E.; Ghosh, A. Ligand Noninnocence in Silver Corroles: A XANES Investigation. *Eur. J. Inorg. Chem.* **2016**, *2016*, 3225-3227.

[62] MacMillan, S. N.; Lancaster, K. M. X-ray Spectroscopic Interrogation of Transition-Metal-Mediated Homogeneous Catalysis: Primer and Case Studies. *ACS Catal*. **2017**, *7*, 1776–1791.

[63] This complex was synthesized as described in: Belghith, Y.; Daran, J.-C.; Nasri, H. Chlorido(pyridine-κN)(5,10,15,20-tetraphenylporphyrinato-$\kappa^4 N$)cobalt(III) chloroform hemisolvate. *Acta Cryst*. **2012**. *E68*, m1104–m1105.

[64] Sarangi, R. X-ray Absorption Near-Edge Spectroscopy in Bioinorganic Chemistry: Application to M–O_2 systems. *Coord. Chem. Rev.* **2013**, *257*, 459-472.

[65] Westre, T. E.; Kennepohl, P.; DeWitt, J. G.; Hedman, B.; Hodgson, K. O.; Solomon, E. I. A Multiplet Analysis of Fe K-Edge 1s→3d Pre-Edge Features of Iron Complexes. *J. Am. Chem. Soc.* **1997**, *119*, 6297-6314.

[66] Glatzel, P.; Bergmann, U. High resolution 1s Core Hole X-ray Spectroscopy in 3d Transition Metal Complexes – Electronic and Structural Information. *Coord. Chem. Rev*. **2005**, *249*, 65–95.

[67] Bauer, M. HERFD-XAS and Valence-to-Core-XES: New Tools to Push the Limits in Research with Hard X-Rays? *Phys. Chem. Chem. Phys*. 2014, **16**, 13827-13837.

[68] The complex was prepared as described in: Madure, P.; Scheidt, W. R. Stereochemistry of Low-Spin Cobalt Porphyrins. 8. α,β,γ,δ-Tetraphenylporphinatocobalt(II). *Inorg. Chem*. **1976**, *15*, 3182–3184.

[69] Vankó, G.; Neisius, T.; Molnár, T.; Renz, F.; Kárpáti, S.; Shukla, A.; de Groot, F. M. Probing the 3d Spin Momentum with X-ray Emission Spectroscopy: The Case of Molecular-Spin Transitions. *J. Phys. Chem. B* **2006**, *110*, 11647-11653.

[70] Pollock, C. J.; Delgado-Jaime, M. U.; Atanasov, M.; Neese, F.; DeBeer, S. Kβ Mainline X-ray Emission Spectroscopy as an Experimental Probe of Metal–Ligand Covalency. *J. Am. Chem. Soc.* **2014**, *136*, 9453-9463.

[71] Pollock, C. J.; DeBeer, S. Insights into the Geometric and Electronic Structure of Transition Metal Centers from Valence-to-Core X-ray Emission Spectroscopy. *Acc. Chem. Res*. **2015**, 48, 2967−2975.

[72] Pollock, C. P.; Delgado-Jaime, M. U.; Atanasov, M.; Neese, F.; DeBeer, S. Kβ Mainline X-ray Emission Spectroscopy as an Experimental Probe of Metal–Ligand Covalency. *J. Am. Chem. Soc*. **2014**, 136, 9453–9463.

[73] Koszarna, B.; Gryko, D. T. Efficient Synthesis of *meso*-Substituted Corroles in a H_2O−MeOH Mixture. *J. Org. Chem*. **2006**, *71*, 3707-3717.

[74] Capar, J.; Berg, S.; Thomas, K. E.; Beavers, C. M.; Gagnon, K. J.; Ghosh, A. Improved Syntheses of *β*-Octabromo-*Meso*-Triarylcorrole Derivatives. *J. Inorg. Biochem*. **2015**, *153*, 162-166.

[75] Sheldrick, G. M. SHELXT - Integrated Space-Group and Crystal-Structure Determination. *Acta Cryst.* **2015**, *71A*, 3-8

[76] Sheldrick, G. M. Crystal Structure Refinement with SHELXL. *Acta Cryst* **2015**, *71C*, 3-8.

[77] The ADF program system uses methods described in: Velde, G. T.; Bickelhaupt, F. M.; Baerends, E. J.; Guerra, C. F.; van Gisbergen, S. J. A.; Snijders, J. G.; Ziegler, T. Chemistry with ADF. *J. Comput. Chem*. **2001**, *22*, 931-967.

[78] Becke, A.D.; Density-functional exchange-energy approximation with correct asymptotic behaviour, *Physical Review A*, **1988**, *38*, 3098-3100.

[79] Lee, C.T.; Yang, W.T.; Parr, R.G. Development of the Colle-Salvetti correlation-energy formula into a functional of the electron-density, *Physical Review B*, **1988**, *37*, 785-789.

[80]. Grimme, S.; Anthony, J.; Ehrlich, S.; Krieg, H. A consistent and accurate *ab initio* parametrization of density functional dispersion correction (DFT-D) for the 94 elements H-Pu *J. Chem. Phys*. **2010**, *132*, Art. no. 154104.

[81] Ravel, B.; Newville, M. ATHENA, ARTEMIS, HEPHAESTUS: Data Analysis for X-ray Absorption Spectroscopy using IFEFFIT. *J. Synchrotron Radiat.* **2005**, *12*, 537–541.

[82] Lee, N.; Petrenko, T.; Bergmann, U.; Neese, F.; DeBeer, S. Probing Valence Orbital Composition with Iron Kβ X-ray Emission Spectroscopy. *J. Am. Chem. Soc.* **2010**, *132*, 9715-9727.

For Table of Contents only:

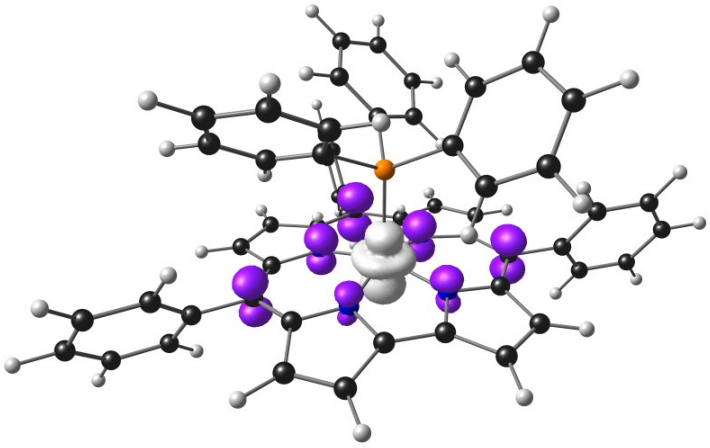

Synopsis: Long thought to be true true low-spin cobalt(III) species, Co-corrole-triphenylphosphine complexes now appear to be noninnocent with partial Co^{II}-$corrole^{\bullet 2-}$ character, underscoring the ubiquity of phenomenon among first-row transition metal corroles.